Human Dicer helicase domain acts as an interaction platform to recruit PKR and dsRNA binding proteins during viral infection

Thomas C. Montavon[1,*], Mathieu Lefèvre[1,*], Morgane Baldaccini[1,*], Erika Girardi[1], Béatrice Chane-Woon-Ming[1], Mélanie Messmer[1], Philippe Hammann[2], Johana Chicher[2], Sébastien Pfeffer[1,‡]

[1] Université de Strasbourg, Architecture et Réactivité de l'ARN, Institut de Biologie Moléculaire et Cellulaire du CNRS, 2 allée Konrad Roentgen, 67084 Strasbourg France

[2] Université de Strasbourg, Institut de Biologie Moléculaire et Cellulaire du CNRS, Plateforme Protéomique Strasbourg – Esplanade, 2 allée Konrad Roentgen, 67084 Strasbourg France

*These authors contributed equally

‡ To whom correspondence should be addressed: spfeffer@unistra.fr

Abstract

The innate immune response against viruses mainly involves type I interferon (IFN) in mammalian cells. The exact contribution of the RNA silencing machinery remains to be established, but several recent studies indicate that the type III ribonuclease DICER can generate viral siRNAs in specific conditions. In addition, it has been proposed that type I IFN and RNA silencing could be mutually exclusive antiviral responses. In order to decipher the implication of DICER during infection of human cells with the Sindbis virus, we determined its interactome by immunoprecipitation and mass spectrometry analysis. Our results show that human DICER specifically interacts with several double-stranded RNA binding proteins and RNA helicases during viral infection. In particular, proteins such as DHX9, ADAR-1 and the protein kinase RNA-activated (PKR) are enriched with DICER in virus-infected cells. We demonstrated the importance of DICER helicase domain in its interaction with PKR and showed that it has functional consequences for the cellular response to viral infection.

34 **Introduction**

35 In mammalian cells, the main antiviral defense system involves the activation of a signaling
36 cascade relying on production of type I interferon (IFN I). This pathway depends on the
37 recognition of extrinsic signals or pathogen associated molecular patterns (PAMPs) by
38 dedicated host receptors. Double-stranded (ds) RNA, which can originate from viral replication
39 or convergent transcription, is a very potent PAMP and can be sensed in the cell by various
40 proteins among which a specific class of DExD/H-box helicases called RIG-I-like receptors
41 (RLRs) (Ivashkiv and Donlin, 2014). RLRs comprise RIG-I, MDA5 and LGP2 and transduce
42 viral infection signals to induce expression of IFN I cytokines that act in autocrine and paracrine
43 fashion. These cytokines then trigger the expression of hundreds of interferon stimulated genes
44 (ISGs) to stop the virus in its tracks (Borden *et al*, 2007). Among those ISGs, dsRNA-activated
45 protein kinase R (PKR) plays an important role in antiviral defense by blocking cellular and
46 viral translation upon direct binding to long dsRNA (Williams, 1999). PKR is a serine-threonine
47 kinase that dimerizes and auto-phosphorylates upon activation. It then phosphorylates
48 numerous cellular targets among which the translation initiation factor eIF2α, which results in
49 the inhibition of cap-dependent translation (Lemaire et al., 2008). Accordingly, translation of
50 many RNA viruses, including alphaviruses, is inhibited by PKR (Fros and Pijlman, 2016;
51 Pfaller et al., 2011; Ryman et al., 2002). PKR is also involved in other cellular pathways
52 including apoptosis, autophagy and cell cycle (Kim et al., 2014; Williams, 1999).

53 RNAi is another evolutionary conserved pathway triggered by long dsRNA sensing
54 (Meister and Tuschl, 2004). One key component in this pathway is the type III ribonuclease
55 DICER, which is also essential for micro (mi)RNA biogenesis (Hutvágner et al., 2001;
56 Wienholds et al., 2003). These small regulatory RNAs are sequentially produced by the two
57 ribonucleases DROSHA and DICER, before being loaded into an Argonaute (AGO) effector
58 protein in order to regulate their target mRNAs (Bartel, 2018). Whatever its substrate, be it long

59 dsRNA or miRNA precursor, DICER relies on interacting with co-factors to be fully functional.
60 In mammalian cells, the TAR-RNA binding protein (TRBP), a dsRNA binding protein
61 (dsRBP), was shown to play a role in the selection of DICER substrates, its stabilization, strand
62 selection and incorporation into AGO2 (Chendrimada et al., 2005). The interaction with TRBP
63 is well characterized and depends on the helicase domain of DICER and the third dsRNA
64 binding domain (dsRBD) of TRBP (Daniels et al., 2009). Another dsRBP, the protein activator
65 of interferon-induced protein kinase R (PACT), was also described as an important cofactor of
66 DICER. Although its function is not fully understood, PACT seems to also participate in
67 miRNA loading and strand selection (Heyam et al., 2015; Kok et al., 2007). via protein-protein
68 interaction between the DICER helicase domain and the third dsRBD of PACT (Lee et al.,
69 2006).

70 It is now common knowledge that RNAi is the main antiviral defense system in several
71 phyla such as plants, arthropods, nematodes (reviewed in (Guo et al., 2019)). However, its exact
72 contribution in the mammalian antiviral response remains unclear (Cullen, 2006; Maillard et
73 al., 2019; tenOever, 2016). Recent studies indicate that a functional antiviral RNAi does exist
74 in mammals in specific cases. A functional antiviral RNAi response was first detected in
75 undifferentiated mouse embryonic stem cells (Maillard et al., 2013) lacking the IFN response,
76 suggesting that these two pathways could be incompatible. Indeed, in mammalian somatic cells
77 deficient for MAVS or IFNAR, two components of the interferon response, an accumulation of
78 DICER-dependent siRNAs derived from exogenous long dsRNA was detected (Maillard et al.,
79 2016). In addition, the RLR LGP2 was found interacting with both DICER and TRBP, blocking
80 respectively siRNA production and miRNA maturation (Takahashi et al., 2018a, 2018b; van
81 der Veen et al., 2018). Moreover, AGO4 was recently showed to be involved in antiviral RNAi
82 against Influenza A virus (IAV), Vesicular stomatitis virus (VSV) and Encephalomyocarditis
83 virus (EMCV) (Adiliaghdam et al., 2020). Finally, viral suppressors of RNAi (VSRs) have been

84 shown to prevent DICER from playing an antiviral role in mammalian cells (Qiu et al., 2020,
85 2017). Nonetheless, several studies reported no detection of viral siRNAs in mammalian
86 somatic cells infected with several viruses (Girardi et al., 2013; Parameswaran et al., 2010;
87 Schuster et al., 2019). In somatic cells, only a helicase-truncated form of human DICER could
88 produce siRNAs from IAV genome(Kennedy et al., 2015), but it also turned out that these
89 siRNAs cannot confer an antiviral state (Tsai et al., 2018).

90 Based on these observations, we decided to study the involvement of DICER during
91 infection of human cells with the Sindbis virus (SINV). SINV is a member of the *Togaviridae*
92 family in the alphavirus genus, which is transmitted by mosquitoes to mammals and can induce
93 arthritogenic as well as encephalitic diseases (Griffin, 2007). It is widely used as a laboratory
94 alphaviruses model as it infects several cell types and replicates to high titers. SINV has a
95 positive stranded RNA genome of about 12 kb, which codes for two polyproteins that give rise
96 to non-structural and structural proteins, including the capsid. Moreover, upon viral replication,
97 a long dsRNA intermediate, which can be sensed by the host antiviral machinery, accumulates.
98 Of note, SINV dsRNA can be cleaved into siRNA in insects as well as in human cells expressing
99 the Drosophila DICER-2 protein (Girardi et al., 2015). Nonetheless, although human DICER
100 has the potential to interact with the viral RNA duplex, we did not find evidence that SINV
101 dsRNA could be processed into siRNAs in somatic mammalian cells (Girardi et al., 2015,
102 2013). We thus hypothesized that specific proteins could interfere with DICER during SINV
103 infection by direct interaction and limit its accessibility and/or activity. To address this
104 hypothesis, we generated HEK 293T cells expressing a tagged version of human DICER that
105 could be immunoprecipitated in mock or SINV-infected cells in order to perform a proteomic
106 analysis of its interactome. Among the proteins co-immunoprecipitated with DICER and that
107 were specifically enriched upon infection, we identified dsRBPs such as ADAR1, DHX9 PACT
108 and PKR. We further validated the direct interaction between DICER and PKR upon SINV

109 infection. We dissected the protein domains necessary for this interaction and we found that
110 DICER helicase domain plays a fundamental role as a recruitment platform for PKR but also
111 for other co-factors. Our results indicate that DICER interactome is highly dynamic and directly
112 link components of RNAi and IFN pathways in modulating the cellular response to viral
113 infection.
114

115 ## Results

116 **Establishment of a HEK 293T cell line expressing FLAG-HA tagged DICER**

117 In order to be able to study the interactome of the human DICER protein during viral infection,
118 we transduced *Dicer* knock-out HEK 293T cells (Hal P. Bogerd et al., 2014) with either a
119 lentiviral construct expressing a FLAG-HA-tagged wild type DICER protein (FHA:DICER) or
120 a construct without insert as a negative control (NoDice). After monoclonal selection of stably
121 transduced cells, we picked a clone that expressed FHA:DICER at levels relatively
122 physiological compared to HEK 293T wild type cells (Fig 1A). Of note, the expression of
123 AGO2, which dropped significantly in NoDice cells, was restored to levels similar to WT cells
124 in the FHA:DICER cell line. We then analyzed the ability of the tagged protein to produce
125 mature miRNAs by northern blot analysis (Fig 1B). The results show that expression of
126 FHA:DICER complements the defect in miRNA production observed in the NoDice cell line.

127 We next characterized the FHA:DICER cell line during SINV infection. We used a
128 modified version of SINV in which the subgenomic promoter has been duplicated to introduce
129 the GFP coding sequence (SINV-GFP) as a readout of viral infection (López et al., 2020). At
130 24 hours post-infection (hpi) and a multiplicity of infection (MOI) of 0.02, the fluorescent GFP
131 signal in FHA:DICER cells was similar to the one observed in HEK 293T cells, while NoDice
132 cells displayed a strong decrease in GFP signal (Fig 1C). Western blot analysis of GFP
133 accumulation (Fig 1D) as well as the analysis of viral particles production by plaque assay (Fig

134 1E) confirmed the epifluorescence microscope observations, *i.e.* a significantly lower
135 accumulation of viral protein and particles in the absence of the DICER protein. In order to
136 check if this phenotype was also visible at a higher MOI and earlier during infection, we
137 infected cells with SINV-GFP at an MOI of 2 for 6 or 16 h. Again, we observed that GFP
138 expression and viral particle production at 16 hpi were similar between HEK 293T and
139 FHA:DICER cells, while they were strongly impaired in NoDice cells (Fig S1A). At 6 hpi, we
140 made similar observations for the expression of the virus-encoded GFP protein (Fig S1B upper
141 and middle panels), but did not see any difference in viral titers between cell lines (Fig S1B
142 lower panel). The latter observation is most likely due to the fact that production of mature viral
143 particles was not yet completed at this early time point.

144 Altogether, these results indicate that the FHA-tagged DICER protein is functional and
145 can be used for proteomics studies. Moreover, these results also show that in our conditions,
146 the loss of DICER protein has an antiviral effect, which is in opposition with previous
147 observations where the replication of various viruses seems to be largely unaffected in DICER
148 knock-out somatic cells (Hal P. Bogerd et al., 2014; Parameswaran et al., 2010; Tsai et al.,
149 2018).

150

151 **Analysis of DICER interactome during SINV infection by mass spectrometry**

152 Our molecular tool being validated, we then focused on determining the interactome of
153 FHA:DICER during SINV infection. We performed an anti-HA immunoprecipitation
154 experiment (HA IP) coupled to label-free LC-MS/MS analysis in FHA:DICER cells either
155 mock-infected or infected for 6 h at an MOI of 2 with SINV-GFP. In parallel, we performed an
156 anti-MYC immunoprecipitation as a negative control (CTL IP). The experiments were
157 performed in technical triplicate in order to have statistically reproducible data for the
158 differential analysis, which was performed using spectral counts. Prior to the detailed analysis

159 of the results, we verified that there was no confounding factor in the experimentation by
160 performing a Principal Component Analysis (PCA). This allowed us to see that the replicates
161 were very homogenous and that the different samples were well separated based on the
162 conditions.

163 To check the specificity of the HA immunoprecipitation, we first compared the proteins
164 identified in the HA IP with the ones identified in the CTL IP in mock-infected cells.
165 Differential expression analysis allowed us to calculate a fold change and an adjusted p-value
166 for each protein identified and to generate a volcano plot representing the differences between
167 HA and CTL IP samples. Applying a fold change threshold of 2 (abs(LogFC) > 1), an adjusted
168 p-value threshold of 0.05 and a cutoff of at least 5 spectral counts in the most abundant
169 condition, we identified 258 proteins differentially immunoprecipitated between the two
170 conditions out of 1318 proteins (Fig 2A and Supp. Table 1). Among these, 123 proteins were
171 specifically enriched in the HA IP. The most enriched protein was DICER, followed by its
172 known co-factors TRBP and PACT (also known as PRKRA) (Chendrimada et al., 2005; Lee et
173 al., 2006). We were also able to retrieve AGO2, indicating that the RISC loading complex has
174 been immunoprecipitated and that proteins retrieved in our HA IP are specific to DICER
175 immunoprecipitation.

176 We next performed the differential expression analysis of proteins retrieved in the HA
177 IP in SINV-GFP compared to mock-infected cells. Among 1342 proteins, 296 were
178 differentially retrieved between conditions (Fig 2B and Supp. Table 2). Of these, 184 proteins,
179 including viral ones, were at least 2-fold enriched in SINV-GFP-infected cells. GO-term
180 analysis showed a significant enrichment in RNA binding proteins including double-stranded
181 RNA binding proteins and RNA helicases (Fig 2C). Among the RNA binding proteins
182 retrieved, the top and most specific DICER interactor is the interferon-induced, double-stranded
183 (ds) RNA-activated protein kinase PKR (also known as E2AK2), which is enriched more than

184 250 times in virus-infected cells (Fig 2B and D). We were also able to identify the dsRNA-
185 specific adenosine deaminase protein ADAR-1 (also known as DSRAD), as well as PACT,
186 which were enriched 5.9 and 4.2 times respectively in SINV-GFP-infected cells compared to
187 mock-infected cells (Fig 2B and D). Among the isolated RNA helicases, we identified the ATP-
188 dependent RNA helicase A protein DHX9, which is implicated in *Alu* element-derived dsRNA
189 regulation and in RISC loading (Aktaş et al., 2017; Robb and Rana, 2007). In order to verify if
190 the observed interactions were specific to SINV we performed the same experiments with
191 another virus of the *Togaviridae* family, the Semliki forest virus (SFV). In this analysis, we
192 were able to retrieve ADAR-1, DHX9, PACT and PKR, specifically enriched in SFV-infected
193 samples (Fig S2 and Supp. Tables 3 and 4). These results show that these interactions can be
194 retrieved in *Togaviridae*-infected cells.
195 Taken together, these results indicate that proteins interacting with DICER in virus-
196 infected cells are involved in dsRNA sensing and/or interferon-induced antiviral response.
197 Because SINV-GFP allows us to have a visual read-out of the infection, we decided to use this
198 virus to continue the analysis.
199
200 **DICER and PKR interact *in vivo* in the cytoplasm during SINV infection**
201 To validate the LC-MS/MS analysis, we performed a co-immunoprecipitation (co-IP) followed
202 by western blot analysis in FHA:DICER cells infected with SINV-GFP at an MOI of 2 for 6 h.
203 Whereas TRBP interacted equally well with FHA:DICER in mock and SINV-GFP-infected
204 cells, ADAR-1, PKR, DHX9 and PACT were only retrieved in the HA IP in SINV-infected
205 cells (Fig 3A). We verified that these interactions could also be observed at a later time in
206 infection by performing the HA IP in FHA:DICER cells infected with SINV-GFP for 24 h at
207 an MOI of 0.02. This allowed us to confirm the specific interactions between DICER and

208 ADAR-1, DHX9, PACT or PKR only in virus-infected cells (Fig S3A), indicating that these
209 interactions occur at an early stage of the infection and remain stable in time.

210 Because of the involvement of PKR in antiviral response (García et al., 2007) and the
211 fact that it shares common co-factors with DICER, namely TRBP and PACT (Haase et al.,
212 2005; Patel et al., 2000), we decided to focus our analysis on the DICER-PKR interaction. To
213 confirm the validity of this interaction, we first performed a reverse co-IP using magnetic beads
214 coupled to anti-PKR antibody in HEK 293T cells infected with SINV-GFP. While PACT
215 interacted as expected with PKR both in mock and in SINV-GFP-infected cells (Fig 3B upper
216 panel), it co-immunoprecipitated with DICER only in virus-infected cells as previously
217 observed (Fig 3B lower panel). In order to determine whether DICER and PKR could interact
218 directly *in vivo*, we set up a bi-molecular fluorescent complementation assay (BiFC) experiment
219 (Lepur et al., 2016). To this end, we fused the N- or C-terminal halves of the Venus protein ($^{N-}$
220 ^{ter}Venus or $^{C-ter}$Venus) to DICER and to PKR but also to TRBP and PACT. Since we showed
221 above that an N-terminally tagged DICER was functional, we fused Venus fragments at the N-
222 terminal end of DICER. For the other three proteins, we fused Venus fragments at the N- or C-
223 terminus and selected the best combination. To avoid interaction with endogenous DICER and
224 PKR proteins, we conducted all BiFC experiments in NoDice/ΔPKR HEK 293T cells (Kennedy
225 et al., 2015). In order to control the BiFC experiment, we chose to exploit the well characterized
226 DICER-TRBP interaction, which is known to occur via the DICER DEAD-Box helicase
227 domain. We therefore used as a positive control the wild-type DICER protein, and as a negative
228 control a truncated version of DICER protein lacking part of this helicase domain and called
229 DICER N1 (Kennedy et al., 2015) (Fig S3B). After confirmation of the expression of the
230 proteins by western blot analysis (Fig S3C), we tested the interactions between DICER and
231 TRBP, PACT or PKR. We co-transfected the Venus constructs for 24 h and then infected cells
232 or not with SINV for 6 h at an MOI of 2. A fluorescent signal was observed both in mock- and

233 SINV-infected cells when $^{N\text{-}ter}$Venus:DICER was co-transfected with any of the three proteins
234 (Fig 3C). Whereas the signal was similar in mock- and virus-infected cells for the DICER-
235 TRBP and DICER-PACT interactions, we observed an increase of the Venus signal for the
236 DICER-PKR interaction in SINV-infected cells compared to mock. These results confirm the
237 previous observations showing an enhanced interaction between DICER and PKR during virus
238 infection. To gain more insight into the subcellular localization of these interactions during
239 SINV infection, we performed the BiFC experiments, fixed the cells and observed them under
240 a confocal microscope. We observed a cytoplasmic signal for DICER-TRBP and DICER-
241 PACT interactions (Fig 3D upper and middle panels), which is in agreement with their
242 canonical localization for the maturation of most miRNAs (Bernstein et al., 2001; Hutvágner
243 et al., 2001). Similarly, co-transfection of DICER and PKR led to a strong Venus signal
244 homogeneously distributed in the cytoplasm (Fig 3D lower panel). As a control and to rule out
245 any aspecific interactions between the different proteins tested, we also monitored the DICER-
246 N1-TRBP interaction by BiFC. As expected, no fluorescent signal was observed in cells co-
247 transfected with $^{N\text{-}ter}$Venus:DICER N1 and TRBP:Venus$^{C\text{-}ter}$ (Fig S3D), confirming that DICER
248 helicase domain is required for its interaction with TRBP (Daniels et al., 2009).
249 Collectively, these results formally confirm that DICER interacts with several RNA
250 helicases and dsRNA-binding proteins in virus-infected cells, among which PKR, and that for
251 the latter this interaction occurs in the cytoplasm.
252
253 **The helicase domain of DICER is required for its interaction with PKR**
254 We next determined the domain of DICER required for its interaction with PKR. Since its
255 helicase domain was previously shown to be involved in the interaction with TRBP and PACT
256 (Daniels et al., 2009; Lee et al., 2006), we speculated that it could also be implicated in binding
257 PKR. To test this hypothesis, we cloned several versions of DICER proteins wholly or partly

258 deleted of the helicase domain (Fig 4A DICER N1 and N3). In addition, we also cloned the
259 helicase domain alone (Fig 4A DICER Hel.) and a DICER variant deleted of its C-terminal
260 dsRNA binding domain (Fig 4A DICER ΔdsRBD) since this domain could also be involved in
261 protein-protein interaction (Doyle et al., 2013; Lambert et al., 2016). We then transfected the
262 different versions of DICER WT and the deletion mutant constructs in NoDice cells. After
263 SINV-GFP infection, whole cell extracts were subjected to HA IP. As for TRBP and to a lesser
264 extent for PACT, we observed that N1 and N3 mutations strongly reduced the binding of
265 DICER with PKR (Fig 4B lanes 2-3 and 7-8). Importantly, we noted that the helicase domain
266 alone could bind PKR, TRBP and PACT (Fig 4B lanes 4 and 9). Moreover, the deletion of the
267 dsRNA binding domain of DICER did not affect its interaction with TRBP, PACT and PKR
268 (Fig 4B lanes 5 and 10). Upon virus infection, PKR is phosphorylated to be activated and exert
269 its antiviral function (Lemaire et al., 2008). Using an antibody targeting the phosphorylated
270 form of PKR (p-PKR), we looked for p-PKR in our co-IP (Fig 4B panel p-PKR). We noticed
271 that only WT DICER and its helicase domain were able to interact with p-PKR (Fig 4B lanes
272 1-6 and 4-9). The fact that DICER ΔdsRBD did not interact with p-PKR (Fig 4B lanes 5-10) is
273 striking but could indicate that the phosphorylation of PKR may induce conformation changes
274 preventing its interaction with some domains of DICER. These results reveal that like for TRBP
275 and PACT, the helicase domain of DICER is required for DICER-PKR/p-PKR interaction
276 during SINV infection.

277 In order to confirm the co-IP experiment, we next decided to perform BiFC experiments
278 using the same conditions as previously. In both mock and SINV-infected cells, only the
279 combinations of DICER WT-PKR and DICER ΔdsRBD-PKR showed a strong Venus signal,
280 while neither DICER N1 nor N3 constructs revealed an interaction with PKR (Fig 4C). In
281 contrast, the DICER Hel. construct did not seem to interact with PKR in mock-infected cells
282 but appeared to do so in SINV-infected cells as a faint Venus signal could be observed. These

283 results therefore confirmed the co-IP observations for the DICER-PKR interaction. In addition,
284 we also performed a BiFC experiment using the different DICER constructs with TRBP or
285 PACT. Altogether, the BiFC results mostly fitted with the co-IP experiment for the DICER-
286 TRBP (Fig S4A) and DICER-PACT (Fig S4B) interactions. TRBP indeed did not seem to
287 interact with the DICER N1 and only slightly with the DICER N3. However, PACT interaction
288 was lost with DICER N1, but not with DICER N3 in mock- and SINV-infected cells (Fig S4B
289 third panel). This result may be explained by the fact that DICER interacts with PACT via the
290 helicase and DUF domains, whereas only the DICER helicase domain is required for its
291 interaction with TRBP (Daniels et al., 2009; Lee et al., 2006). In agreement, the Venus signal
292 observed between the DICER Hel. and PACT seemed weaker than the one we observed with
293 TRBP (Fig S4A and B fourth panels).

294 Taken together these results indicate that DICER interacts with both PKR and its
295 phosphorylated form during SINV infection and that this interaction requires the helicase
296 domain of DICER.

297

298 **Functional importance of DICER helicase domain during SINV infection**

299 We finally sought to study the functional role of DICER-PKR interaction during viral infection.
300 For this purpose, we decided to use DICER N1 to study SINV infection. To do so, we generated
301 by lentiviral transduction NoDice HEK 293T cells stably expressing FHA-tagged DICER N1
302 (FHA:DICER N1). As for the FHA:DICER cell line, we first selected a clone expressing the
303 tagged DICER N1 at a level similar level to the endogenous one in HEK 293T cells (Fig 5A).
304 DICER N1 protein has been shown to still be able to produce miRNAs (Kennedy et al., 2015).
305 We thus verified by northern blot analysis the capacity of the FHA:DICER N1 cell line to
306 produce mature miRNAs. The results indicate that indeed DICER N1 is still able to process
307 miRNAs similarly to WT DICER in HEK 293T and FHA:DICER cells, thereby validating the

308 functionality of the tagged protein (Fig 5B). We next infected HEK 293T, NoDice,
309 FHA:DICER and FHA:DICER N1 cells with SINV-GFP and measured virus accumulation by
310 assessing GFP protein level and virion production (Fig 5C and D and E). As in NoDice cells,
311 the GFP protein level was drastically reduced in FHA:DICER N1 cells compared to
312 FHA:DICER and HEK 293T cells (Fig 5C and D). In addition, we observed a statistically
313 significant reduction in viral titer in both NoDice and FHA:DICER N1 cells compared to HEK
314 293T or FHA:DICER cells (Fig 5E). This indicates that FHA:DICER N1, lacking the Hel 1 and
315 Hel 2i domains, is not able to restore the defects observed in NoDice cells.

316 Moreover, these results show that the antiviral effect observed in NoDice cells is
317 probably not due to a default in miRNA production but more likely to a loss of interaction
318 between DICER and PKR.

319

320 **Discussion**

321 The role of DICER in antiviral defense in human cells remains a topic of intense discussion
322 (Cullen et al., 2013; Maillard et al., 2013, 2019; Cullen, 2017). In particular there have been
323 contradictory reports regarding its capacity to produce siRNAs from viral RNAs (Hal P. Bogerd
324 et al., 2014; Parameswaran et al., 2010; Donaszi-Ivanov et al., 2013; Backes et al., 2014). These
325 observations could be due to the fact that several mammalian viruses potentially encode VSR
326 proteins, thereby masking the effect of RNAi (Li et al., 2016, 2013; Maillard et al., 2013; Qiu
327 et al., 2020, 2017). Another putative but non-exclusive explanation could be that there is a
328 mutual regulation of type I IFN and RNAi pathways (Berkhout, 2018; Takahashi and Ui-Tei,
329 2020). Thus, it has already been shown that PACT can regulate MDA5 and RIG-I during virus
330 infection and therefore the induction of type I IFN response (Kok et al., 2011; Lui et al., 2017).
331 To date, it is not clear whether the activity of the DICER protein as well could be regulated by
332 potential interactors, or inversely whether it could itself modulate the activity of proteins

333 involved in the IFN pathway. To answer this question, we determined the changes in the
334 interactome of human DICER upon SINV and SFV infection. This analysis allowed us to reveal
335 that a lot of proteins associating with DICER during viral infection are dsRNA-binding proteins
336 and RNA helicases. A number of these proteins are known to be involved in antiviral defense
337 pathways, thereby indicating the possible formation of one or several complexes between
338 DICER and these proteins, which are very likely brought together by the accumulation of
339 dsRNA during virus infection.

340 Among these proteins, we chose to focus on the well-known ISG PKR, which is
341 involved in many cellular pathways such as apoptosis, cellular differentiation, development and
342 antiviral defense (Clemens, 1997; Gal-Ben-Ari et al., 2018; Kim et al., 2014; Lemaire et al.,
343 2008). PKR is one of the main actors of the Integrative Stress Response (ISR) in human cells,
344 and its activation or inhibition needs to be tightly regulated in order to have a properly balanced
345 response to stress. Our results indicate that DICER interacts via its helicase domain with PKR
346 in the cytoplasm during SINV infection. The helicase domain of DICER, which is also required
347 for its interaction with TRBP and PACT, belongs to the helicase superfamily 2, which is also
348 found in RLRs such as RIG-I, MDA5 or LGP2 (Ahmad and Hur, 2015; Fairman-Williams et
349 al., 2010). These proteins act as sensors of viral infection and through the activation of proteins
350 such as MAVS, mediate the induction of type I IFN pathway (Ahmad and Hur, 2015). We
351 hypothesize that even though the human DICER helicase has evolved mainly to act in
352 miRNA/siRNA pathway, it still retained the capacity to act as an RLR. However, as opposed
353 to RIG-I and MDA5, our data suggest that DICER would act more as an inhibitor rather than
354 inducer of the immune response. Therefore, we propose that this domain serves as a platform
355 for the recruitment of different proteins to diversify the function of DICER.

356 One such regulatory effect appears to be on the antiviral activity of PKR, as cells lacking
357 DICER or expressing a truncated form of DICER unable to interact with PKR are less

358 permissive to SINV infection. This is in agreement with previous observations that ectopic
359 expression of the *Drosophila* DICER2 protein in human cells perturbs IFN signaling pathways
360 and antagonizes PKR-mediated antiviral immunity (Girardi et al., 2015). The exact mechanism
361 involved is still unclear and will require further work, but it seems that it is not solely due to a
362 competition of the two proteins for dsRNA binding. Indeed, DICER and PKR interact in BiFC
363 assay, a technique that favors the detection of direct interactions (Lepur et al., 2016). Moreover,
364 the DICER helicase domain alone can interact with PKR suggesting that this interaction is
365 independent of the dsRNA substrates. Most of the time, the inhibition of PKR activity relies on
366 its inhibition to bind to dsRNA or to auto-phosphorylate. For example, the human tRNA-
367 dihydrouridine synthase 2 (hDus2) binds the first dsRBD of PKR and prevents its activation
368 (Mittelstadt et al., 2008). TRBP binds dsRNAs but also PKR directly hindering its dimerization.
369 In normal condition, TRBP is also associated with PACT thus preventing PKR activation by
370 PACT (Park et al., 1994; Nakamura et al., 2015; Daher et al., 2009; Singh et al., 2011). Since
371 we showed that DICER can bind the activated phospho-PKR, we hypothesize that this
372 interaction does not result in the inhibition of PKR autophosphorylation. Therefore, one
373 possibility could be that DICER interaction with PKR prevents the latter from acting upon some
374 of its targets, which remain to be identified, to fine-tune the antiviral response.

375 As of now, we cannot formally rule out that the effect of DICER on PKR is mediated
376 by other proteins. TRBP and PACT have been shown to regulate PKR activity, the former
377 normally acting as a repressor and the latter as an activator (Nakamura et al., 2015; Patel et al.,
378 2000; Singh et al., 2011). Interestingly, in lymphocytic Jurkat cells infected by HIV-1, PACT
379 can also act as a repressor of PKR (Clerzius et al., 2013). It is thus tempting to speculate that
380 these two proteins participate in the formation of the DICER-PKR complex. However, our
381 results show that this may not necessarily be the case. Indeed, in the BiFC experiment, the

382 DICER N3 mutant still interacted with PACT but not with PKR indicating that PACT binding
383 is not sufficient to confer the association with PKR.

384 Besides PKR, other proteins were specifically enriched upon viral infection in the
385 DICER IP. These are also interesting candidates to explain the putative regulatory role of
386 DICER. Among these proteins, DHX9 and ADAR-1 are especially intriguing. DHX9, also
387 known as RNA helicase A (RHA), associates with RISC, helping the RISC loading (Robb and
388 Rana, 2007). Moreover, DHX9 is directly involved in removing toxic dsRNAs from the cell to
389 prevent their processing by DICER (Aktaş et al., 2017). It has also been implicated in HIV-1
390 replication and knockdown of DXH9 leads to the production of less infectious HIV-1 virions
391 (Li et al., 1999; Fujii et al., 2001; Roy et al., 2006). Finally, DXH9 interacts with and is
392 phosphorylated by PKR in mouse embryonic fibroblasts. This phosphorylation precludes the
393 association of DHX9 with RNA, thus inhibiting its proviral effect (Sadler et al., 2009). In light
394 of these observations and ours, we can speculate that the inhibitory effect of DICER on PKR
395 activity could also be linked to DHX9 phosphorylation. ADAR-1 is one of the well-known
396 RNA-editing factors (Herbert et al., 1997). ADAR-1 is linked to both miRNA biogenesis (Iizasa
397 et al., 2010; Ota et al., 2013; Yang et al., 2006, p. 1) and virus infection. Indeed, ADAR-1 has
398 an antiviral effect against Influenza virus, but most of the time, its depletion leads to a decrease
399 of the viral titer, as was reported for VSV or HIV-1 (Li et al., 2010; Samuel, 2011). It has been
400 shown that ADAR-1 and PKR interact directly during HIV-1 infection. This interaction triggers
401 the inhibition of PKR activation, and thus a reduction of eIF2α phosphorylation leading to an
402 increase of virus replication (Pfaller et al., 2011; Clerzius et al., 2009). Interestingly, over-
403 expression of ADAR-1 enhances drastically the replication of the alphaviruses Chikungunya
404 virus (CHIKV), and Venezuelan equine encephalitis virus (VEEV) most likely by interfering
405 with the IFN induction (Schoggins et al., 2011).

406 Deciphering the exact role of human DICER protein during virus infection is a
407 challenging task and additional studies will be required to get a global picture. Nonetheless, by
408 assessing the interactome of this protein during SINV infection, we have unveiled a new role
409 for the helicase domain of DICER in regulating the cellular response to viral infection.
410

411 ## Material and methods

412 **Plasmids, cloning and mutagenesis**

413 Plasmids used for BiFC experiments were a gift from Dr. Oliver Vugrek from the Ruđer
414 Bošković Institute and described in . The cDNAs of TRBP, PACT and PKR were respectively
415 amplified from (pcDNA-TRBP Addgene #15666) (Kok et al., 2007), (pcDNA-PACT Addgene
416 #15667) (Kok et al., 2007), (pSB819-PKR-hum Addgene #20030) (Elde et al., 2009), and
417 cloned into the four pBiFC vectors by Gateway recombination. DICER N1, N3 Hel. and
418 ΔdsRBD were generated by PCR mutagenesis from pDONR-DICER described in (Girardi et
419 al., 2015) and cloned into the four pBiFC and pDEST-FHA vectors by Gateway recombination.
420 plenti6 FHA-V5 vector was modified from plenti6-V5 gateway vector (Thermo Fisher
421 scientific V49610) by Gibson cloning. DICER WT, N1 from pDONOR plasmids were cloned
422 into plenti6 FHA-V5 by Gateway recombination. All primers used are listed in Supp. Table 5.
423

424 **Cell lines**

425 HEK 293T, HEK 293T/NoDice, and HEK 293T/NoDiceΔPKR cell lines were a gift from Pr.
426 Bryan Cullen and described in (H. P. Bogerd et al., 2014; Kennedy et al., 2015).
427

428 **Cell culture and transfection**

429 Cells were maintained in Dulbecco's modified Eagle medium (DMEM, Gibco) supplemented
430 with 10% fetal bovine serum (FBS, Clontech) in a humidified atmosphere of 5% CO_2 at 37°C.

431 Transfection was performed using Lipofectamine 2000 (Thermofisher) according to the
432 manufacturer's instructions.
433
434 **Lentivirus production and generation of stable cell lines**
435 The lentiviral supernatant from single transfer vector was produced by transfecting HEK293T
436 cells (ATCC® CRL-3216™) with 20 µg the transfer vector, 15 µg of pMDLg/p RRE and 10
437 µg of pRSV-Rev packaging plasmids (Addgene # 12251 and Addgene #12253) and the pVSV
438 envelope plasmid (Addgene #8454) using Lipofectamine 2000 (Thermofisher) reagent
439 according to manufacturer protocol. Standard DMEM (GIBCO) medium supplemented with
440 10% Fetal bovine serum (FBS, Gibco) and 100 U/mL of penicillin-Streptomycin (Gibco) was
441 used for growing HEK293T cells and for lentivirus production. One 10 cm plate of HEK293T
442 cells at 70-80% confluency was used for the transfection. The medium was replaced 8 hours
443 post-transfection. After 48 hours the medium containing viral particles was collected and
444 filtered through a 0.45μm PES filter. The supernatant was directly used for transfection or
445 stored at -80°C. A 6 well plate of HEK 293T/NoDice cells at 80% confluency was transduced
446 using 600 μL of lentiviral supernatant either expressing FHADICER, N1 or empty vector,
447 supplemented with 4 ug/mL polybrene (Sigma) for 6 hours. The transduction media was then
448 changed with fresh DMEM for 24 hours and the resistant cells clones were selected for about
449 6 weeks with blasticidin (15 µg/mL) and subsequently maintained under blasticidin selection.
450
451 **Viral stocks, virus infection**
452 Viral stocks of SINV or SINV-GFP were produced as described in (Girardi et al., 2015). Cells
453 were infected with SINV or SINV-GFP at an MOI of 0.02 or 2 and samples were collected at
454 different time points as indicated in the figure legends.
455

456 **Analysis of viral titer by plaque assay**

457 Vero R cells were seeded in 96-well plates format and were infected with 10-fold serial
458 dilutions infection supernatants for 1 h. Afterwards, the inoculum was removed, and cells were
459 cultured in 2.5% carboxymethyl cellulose for 72 h at 37°C in a humidified atmosphere of 5%
460 CO_2. Plaques were counted manually under the microscope and viral titer was calculated
461 according to the formula: *PFU/mL = #plaques/ (Dilution*Volume of inoculum)*

462

463 **Western blot analysis**

464 Proteins were extracted from cells and homogenized in 350 µL of lysis buffer (50 mM Tris-
465 HCl pH 7.5, 150 mM NaCl, 5 mM EDTA, 1% Triton X-100, 0.5% SDS and Protease Inhibitor
466 Cocktail (complete Mini; Sigma Aldrich)). Proteins were quantified by the Bradford method
467 and 20 to 30 µg of total protein extract were loaded on 4-20% Mini-PROTEAN® TGX™
468 Precast Gels (Bio-Rad). After transfer onto nitrocellulose membrane, equal loading was verified
469 by Ponceau staining. For PVDF membrane, equal loading was verified by Coomassie staining
470 after transfer and blotting. Membranes were blocked in 5% milk and probed with the following
471 antibodies: anti-hDicer (1:500, F10 Santa Cruz sc-136979), anti-TRBP (1:500, D-5 Santa Cruz
472 sc-514124), anti-PKR (1:2500, Abcam ab32506), anti-PACT (1:500, Abcam, ab75749), anti-
473 HA (1:10000, Sigma, H9658), anti-DHX9 (1:500, Abcam ab26271), anti-p-eIF2a (1:1000, Ser-
474 52 Santa Cruz sc-601670), anti-hADAR-1 (1:500 Santa Cruz sc-271854) anti-p-PKR (1:1000
475 Abcam ab81303) anti-GFP (1:10000, Roche 11814460001) and anti-Tubulin (1:10000, Sigma
476 T6557). Detection was performed using Chemiluminescent Substrate (Pierce, Thermofisher)
477 and visualized on a Fusion FX imaging system (Vilber).

478

479 **RNA extraction and northern blot analysis**

480 Total RNA was extracted using Tri-Reagent Solution (Fisher Scientific; MRC, Inc) according
481 to the manufacturer's instructions. Northern blotting was performed on 10 μg of total RNA.
482 RNA was resolved on a 12% urea-acrylamide gel, transferred onto Hybond-NX membrane (GE
483 Healthcare). RNAs were then chemically cross-linked to the membrane during 90 min at 65°C
484 using 1-ethyl-3-[3-dimethylaminopropyl]carbodiimide hydrochloride (EDC) (Sigma Aldrich).
485 Membranes were prehybridized for 30 min in PerfectHyb™ plus (Sigma Aldrich) at 50°C.
486 Probes consisting of oligodeoxyribonucleotides (see Supplementary Table 2) were 5′-end
487 labeled using T4 polynucleotide kinase (Thermofisher) with 25 μCi of [γ-32P]dATP. The
488 labeled probe was hybridized to the blot overnight at 50°C. The blot was then washed twice at
489 50°C for 20 min (5× SSC/0.1% SDS), followed by an additional wash (1× SSC/0.1% SDS) for
490 5 min. Northern blots were exposed to phosphorimager plates and scanned using a Bioimager
491 FLA-7000 (Fuji).
492
493 **Immunoprecipitation**
494 Immunoprecipitation experiments were carried out either on tagged proteins or on endogenous
495 proteins.
496 *Tagged proteins*: Cells were harvested, washed twice with ice-cold 1× PBS (Gibco®, Life
497 Technologies), and resuspended in 550 μL of lysis buffer (50 mM Tris-HCl pH 7.5, 140 mM
498 NaCl, 1.5 mM $MgCl_2$, 0.1% NP-40), supplemented with Complete-EDTA-free Protease
499 Inhibitor Cocktail (complete Mini; Sigma Aldrich). Cells were lysed by 30 min incubation on
500 ice and debris were removed by 15 min centrifugation at 2000 g and 4°C. An aliquot of the
501 cleared lysates (50 μL) was kept aside as protein Input. Samples were divided into equal parts
502 (250 μL each) and incubated with 15 μL of magnetic microparticles coated with monoclonal
503 HA or MYC antibodies (MACS purification system, Miltenyi Biotech) at 4°C for 1 h under
504 rotation (10 rpm). Samples were passed through *μ* Columns (MACS purification system,

505 Miltenyi Biotech). The *μ* Columns were then washed 3 times with 200 μL of lysis buffer and 1
506 time with 100 μL of washing buffer (20 mM Tris-HCl pH 7.5). To elute the immunoprecipitated
507 proteins, 95°C pre-warmed 2x Western blot loading buffer (10% glycerol, 4% SDS, 62.5 mM
508 Tris-HCl pH 6.8, 5% (v/v) 2-β-mercaptoethanol, Bromophenol Blue) was passed through the
509 *μ* Columns. Proteins were analyzed by western blotting or by mass spectrometry.
510 *Endogenous proteins*: The day before immunoprecipitation, magnetic DynaBeads protein G
511 (Invitrogen) were prepared: briefly, 160 μL of magnetic DynaBeads protein G (Invitrogen)
512 were washed three times with lysis buffer (50 mM Tris-HCl pH 7.5, 150 mM NaCl, 5 mM
513 EDTA, 1% Triton X-100, 0.5% SDS). The beads were then incubated with 4 μg of BSA for 1
514 h under agitation at room temperature. An aliquot of beads (40 μL) was kept for preclearing
515 step. The remaining beads were incubated either with 6 μg of PKR antibody or control IgG
516 overnight at 4°C under rotation.
517 For the IP: Cells were harvested, washed twice with ice-cold 1× PBS (Gibco®, Life
518 Technologies) and resuspended in 1 mL of lysis buffer (50 mM Tris-HCl pH 7.5, 150 mM
519 NaCl, 5 mM EDTA, 1% Triton X-100, 0.5% SDS) supplemented with Complete-EDTA-free
520 Protease Inhibitor Cocktail (complete Mini; Sigma Aldrich). Cells were lysed by three 15 s
521 sonication steps followed by 30 min incubation on ice and debris were removed by 15 min
522 centrifugation at 16000 g and 4°C. After centrifugation, an aliquot was kept aside as protein
523 Input. Samples were incubated with beads alone for preclearing step for 1 h at 4°C on wheel.
524 Samples were then put on magnetic racks and the supernatant transferred on new tubes
525 containing either beads coupled to PKR antibody or to control IgG. Samples were incubated on
526 wheel for 3 h at 4°C. After incubation, samples were put on magnetic racks and beads were
527 washed three times with lysis buffer. After removal of supernatant, beads were eluted with 2x
528 western blot loading buffer and incubated for 10 min at 95°C under agitation. Proteins were
529 analyzed by western blotting.

530 **BiFC assay**

531 Experiments were carried out in two different ways. For non-fixed cells, NoDice ΔPKR cells
532 were seeded at the density of 1.2 x 10^5 cells per well in a 24-well plate. After 16 hours, cells
533 were transfected with equimolar quantities of each plasmid forming BiFC couples. After 24
534 hours, cells were infected with SINV at an MOI of 2 and pictures were taken 6 hours post-
535 infection using ZOE fluorescent cell imager (Bio-Rad). Proteins were collected with lysis buffer
536 (50 mM Tris-HCl pH 7.5, SDS 0.05%, Triton 1%, 5 mM EDTA, 150 mM NaCl) supplemented
537 with Complete-EDTA-free Protease Inhibitor Cocktail (complete Mini; Sigma Aldrich), and
538 subjected to western blot analysis. For fixed cells, NoDice/ΔPKR cells were seeded at the
539 density of 8.10^4 cells per well in 8-well Millicell® EZ Slides (Merck Millipore), transfected
540 and infected as described previously. At 6 hours post-infection, cells were fixed with 4%
541 formaldehyde and 0.2% glutaraldehyde for 10 min. Cells were then washed with 1 × PBS
542 (Gibco®, Life Technologies) and stained with 10 μg/μL DAPI in 1 × PBS solution (Invitrogen)
543 for 5 min. Fixed cells were mounted on a glass slide with Fluoromount-G mounting media
544 (Southern Biotech). Images were acquired using confocal LSM780 (Zeiss) inverted microscope
545 with an argon laser (514x nm) and with ×40 immersion oil objective. All pictures obtained
546 from BiFC experiments were treated using FigureJ software (NIH).

547

548 **Mass spectrometry analysis**

549 Protein extracts were prepared for mass spectrometry as described in a previous study (Chicois
550 et al., 2018). Each sample was precipitated with 0.1 M ammonium acetate in 100% methanol,
551 and proteins were resuspended in 50 mM ammonium bicarbonate. After a reduction-alkylation
552 step (dithiothreitol 5 mM – iodoacetamide 10 mM), proteins were digested overnight with
553 sequencing-grade porcine trypsin (1:25, w/w, Promega, Fitchburg, MA, USA). The resulting
554 vacuum-dried peptides were resuspended in water containing 0.1% (v/v) formic acid (solvent

555 A). One sixth of the peptide mixtures were analyzed by nanoLC-MS/MS an Easy-nanoLC-1000
556 system coupled to a Q-Exactive Plus mass spectrometer (Thermo-Fisher Scientific, USA)
557 operating in positive mode. Five microliters of each sample were loaded on a C-18 precolumn
558 (75 µm ID × 20 mm nanoViper, 3 μm Acclaim PepMap; Thermo) coupled with the analytical
559 C18 analytical column (75 µm ID × 25 cm nanoViper, 3 μm Acclaim PepMap; Thermo).
560 Peptides were eluted with a 160 min gradient of 0.1% formic acid in acetonitrile at 300 nL/min.
561 The Q-Exactive Plus was operated in data-dependent acquisition mode (DDA) with Xcalibur
562 software (Thermo-Fisher Scientific). Survey MS scans were acquired at a resolution of 70K at
563 200 m/z (mass range 350-1250), with a maximum injection time of 20 ms and an automatic
564 gain control (AGC) set to 3e6. Up to 10 of the most intense multiply charged ions (≥2) were
565 selected for fragmentation with a maximum injection time of 100 ms, an AGC set at 1e5 and a
566 resolution of 17.5K. A dynamic exclusion time of 20 s was applied during the peak selection
567 process.
568
569 **Database search and mass-spectrometry data post-processing**
570 Data were searched against a database containing Human and Viruses UniProtKB sequences
571 with a decoy strategy (GFP, Human and Sindbis Virus SwissProt sequences as well as Semliki
572 Forest Virus SwissProt and TrEMBL sequences (releases from January 2017, 40439
573 sequences)). Peptides were identified with Mascot algorithm (version 2.3, Matrix Science,
574 London, UK) with the following search parameters: carbamidomethylation of cysteine was set
575 as fixed modification; N-terminal protein acetylation, phosphorylation of serine / threonine /
576 tyrosine and oxidation of methionine were set as variable modifications; tryptic specificity with
577 up to three missed cleavages was used. The mass tolerances in MS and MS/MS were set to 10
578 ppm and 0.02 Da respectively, and the instrument configuration was specified as "ESI-Trap".
579 The resulting .dat Mascot files were then imported into Proline v1.4 package

580 (http://proline.profiproteomics.fr/) for post-processing. Proteins were validated with Mascot
581 pretty rank equal to 1, 1% FDR on both peptide spectrum matches (PSM) and protein sets
582 (based on score). The total number of MS/MS fragmentation spectra (Spectral count or SpC)
583 was used for subsequent protein quantification in the different samples.
584

585 **Exploratory and differential expression analysis of LC-MS/MS data**

586 Mass spectrometry data obtained for each sample were stored in a local MongoDB database
587 and subsequently analyzed through a Shiny Application built upon the R/Bioconductor
588 packages msmsEDA (Gregori J, Sanchez A, Villanueva J (2014). msmsEDA: Exploratory Data
589 Analysis of LC-MS/MS data by spectral counts. R/Bioconductor package version 1.22.0) and
590 msmsTests (Gregori J, Sanchez A, Villanueva J (2013). msmsTests: LC-MS/MS Differential
591 Expression Tests. R/Bioconductor package version 1.22.0). Exploratory data analyses of LC-
592 MS/MS data were thus conducted, and differential expression tests were performed using a
593 negative binomial regression model. The p-values were adjusted with FDR control by the
594 Benjamini-Hochberg method and the following criteria were used to define differentially
595 expressed proteins: an adjusted p-value < 0.05, a minimum of 5 SpC in the most abundant
596 condition, and a minimum fold change of 2 (abs(LogFC) > 1).
597

598 **Data availability**

599 The mass spectrometry proteomics data have been deposited to the ProteomeXchange
600 Consortium via the PRIDE (Perez-Riverol et al., 2019) partner repository with the dataset
601 identifier PXD019093 and 10.6019/PXD019093.
602
603
604

605 ## Acknowledgments

606 The authors would like to thank members of the Pfeffer laboratory for discussion, Pr. Bryan
607 Cullen for the kind gift of the HEK293T NoDice and NoDice/ΔPKR cell lines and Dr. Oliver
608 Vugrek for the BiFC plasmids.
609 This work was funded by the European Research Council (ERC-CoG-647455 RegulRNA) and
610 was performed under the framework of the LABEX: ANR-10-LABX-0036_NETRNA, which
611 benefits from a funding from the state managed by the French National Research Agency as
612 part of the Investments for the future program. This work has also received funding from the
613 People Programme (Marie Curie Actions) of the European Union's Seventh Framework
614 Program (FP7/2007-2013) under REA grant agreement n° PCOFUND-GA-2013-609102,
615 through the PRESTIGE program coordinated by Campus France (to EG), and from the French
616 Minister for Higher Education, Research and Innovation (PhD contract to MB). The mass
617 spectrometry instrumentation was funded by the University of Strasbourg, IdEx "Equipement
618 mi-lourd" 2015.

619

620 ## Authors contributions

621 SP and ML conceived the project. TCM, ML, EG and SP designed the work. TCM, ML, MB,
622 EG and MM performed the experiments and analyzed the results. PH and JC performed the
623 mass spectrometry analysis. BCWM designed softwares and analyzed the mass spectrometry
624 results. SP coordinated the work and assured funding. TCM, MB and SP wrote the manuscript
625 with input from the other authors. All authors reviewed and approved the final manuscript.

626

627 **References**

628 Adiliaghdam F, Basavappa M, Saunders TL, Harjanto D, Prior JT, Cronkite DA, Papavasiliou
629 N, Jeffrey KL. 2020. A Requirement for Argonaute 4 in Mammalian Antiviral Defense.
630 *Cell Rep* **30**:1690-1701.e4. doi:10.1016/j.celrep.2020.01.021

631 Ahmad S, Hur S. 2015. Helicases in Antiviral Immunity: Dual Properties as Sensors and
632 Effectors. *Trends Biochem Sci* **40**:576–585. doi:10.1016/j.tibs.2015.08.001

633 Aktaş T, Avşar Ilık İ, Maticzka D, Bhardwaj V, Pessoa Rodrigues C, Mittler G, Manke T,
634 Backofen R, Akhtar A. 2017. DHX9 suppresses RNA processing defects originating
635 from the Alu invasion of the human genome. *Nature* **544**:115–119.
636 doi:10.1038/nature21715

637 Backes S, Langlois RA, Schmid S, Varble A, Shim JV, Sachs D, tenOever BR. 2014. The
638 Mammalian Response to Virus Infection Is Independent of Small RNA Silencing. *Cell*
639 *Rep* **8**:114–125. doi:10.1016/j.celrep.2014.05.038

640 Bartel DP. 2018. Metazoan MicroRNAs. *Cell* **173**:20–51. doi:10.1016/j.cell.2018.03.006

641 Berkhout B. 2018. RNAi-mediated antiviral immunity in mammals. *Curr Opin Virol*,
642 Engineering for viral resistance • Viruses and cancer **32**:9–14.
643 doi:10.1016/j.coviro.2018.07.008

644 Bernstein E, Caudy AA, Hammond SM, Hannon GJ. 2001. Role for a bidentate ribonuclease
645 in the initiation step of RNA interference. *Nature* **409**:363–6.

646 Bogerd Hal P., Skalsky RL, Kennedy EM, Furuse Y, Whisnant AW, Flores O, Schultz KLW,
647 Putnam N, Barrows NJ, Sherry B, Scholle F, Garcia-Blanco MA, Griffin DE, Cullen
648 BR. 2014. Replication of many human viruses is refractory to inhibition by endogenous
649 cellular microRNAs. *J Virol* **88**:8065–8076. doi:10.1128/JVI.00985-14

650 Bogerd H. P., Whisnant AW, Kennedy EM, Flores O, Cullen BR. 2014. Derivation and
651 characterization of Dicer- and microRNA-deficient human cells. *RNA* **20**:923–937.
652 doi:10.1261/rna.044545.114

653 Borden EC, Sen GC, Uze G, Silverman RH, Ransohoff RM, Foster GR, Stark GR. 2007.
654 Interferons at age 50: past, current and future impact on biomedicine. *Nat Rev Drug*
655 *Discov* **6**:975–990. doi:10.1038/nrd2422

656 Chen EY, Tan CM, Kou Y, Duan Q, Wang Z, Meirelles GV, Clark NR, Ma'ayan A. 2013.
657 Enrichr: interactive and collaborative HTML5 gene list enrichment analysis tool. *BMC*
658 *Bioinformatics* **14**:128. doi:10.1186/1471-2105-14-128

659 Chendrimada TP, Gregory RI, Kumaraswamy E, Norman J, Cooch N, Nishikura K, Shiekhattar
660 R. 2005. TRBP recruits the Dicer complex to Ago2 for microRNA processing and gene
661 silencing. *Nature* **436**:740–4.
662 Chicois C, Scheer H, Garcia S, Zuber H, Mutterer J, Chicher J, Hammann P, Gagliardi D,
663 Garcia D. 2018. The UPF1 interactome reveals interaction networks between RNA
664 degradation and translation repression factors in Arabidopsis. *Plant J* **96**:119–132.
665 doi:10.1111/tpj.14022
666 Clemens MJ. 1997. PKR-a protein kinase regulated by double-stranded RNA. *Int J Biochem*
667 *Cell Biol* **29**:945–9.
668 Clerzius G, Gélinas J-F, Daher A, Bonnet M, Meurs EF, Gatignol A. 2009. ADAR1 interacts
669 with PKR during human immunodeficiency virus infection of lymphocytes and
670 contributes to viral replication. *J Virol* **83**:10119–10128. doi:10.1128/JVI.02457-08
671 Clerzius G, Shaw E, Daher A, Burugu S, Gélinas J-F, Ear T, Sinck L, Routy J-P, Mouland AJ,
672 Patel RC, Gatignol A. 2013. The PKR activator, PACT, becomes a PKR inhibitor during
673 HIV-1 replication. *Retrovirology* **10**:96. doi:10.1186/1742-4690-10-96
674 Cullen BR. 2017. RNA Interference in Mammals: The Virus Strikes Back. *Immunity* **46**:970–
675 972. doi:10.1016/j.immuni.2017.05.004
676 Cullen BR. 2006. Is RNA interference involved in intrinsic antiviral immunity in mammals?
677 *Nat Immunol* **7**:563–7.
678 Cullen BR, Cherry S, tenOever BR. 2013. Is RNA Interference a Physiologically Relevant
679 Innate Antiviral Immune Response in Mammals? *Cell Host Microbe* **14**:374–378.
680 doi:10.1016/j.chom.2013.09.011
681 Daher A, Laraki G, Singh M, Melendez-Peña CE, Bannwarth S, Peters AHFM, Meurs EF,
682 Braun RE, Patel RC, Gatignol A. 2009. TRBP control of PACT-induced
683 phosphorylation of protein kinase R is reversed by stress. *Mol Cell Biol* **29**:254–265.
684 doi:10.1128/MCB.01030-08
685 Daniels SM, Melendez-Peña CE, Scarborough RJ, Daher A, Christensen HS, El Far M, Purcell
686 DFJ, Lainé S, Gatignol A. 2009. Characterization of the TRBP domain required for
687 dicer interaction and function in RNA interference. *BMC Mol Biol* **10**:38.
688 doi:10.1186/1471-2199-10-38
689 Donaszi-Ivanov A, Mohorianu I, Dalmay T, Powell PP. 2013. Small RNA Analysis in Sindbis
690 Virus Infected Human HEK293 Cells. *PLoS ONE* **8**:e84070.
691 doi:10.1371/journal.pone.0084070

692 Doyle M, Badertscher L, Jaskiewicz L, Güttinger S, Jurado S, Hugenschmidt T, Kutay U,
693 Filipowicz W. 2013. The double-stranded RNA binding domain of human Dicer
694 functions as a nuclear localization signal. *RNA N Y N* **19**:1238–1252.
695 doi:10.1261/rna.039255.113
696 Elde NC, Child SJ, Geballe AP, Malik HS. 2009. Protein kinase R reveals an evolutionary
697 model for defeating viral mimicry. *Nature* **457**:485–489. doi:10.1038/nature07529
698 Fairman-Williams ME, Guenther U-P, Jankowsky E. 2010. SF1 and SF2 helicases: family
699 matters. *Curr Opin Struct Biol* **20**:313–324. doi:10.1016/j.sbi.2010.03.011
700 Fros JJ, Pijlman GP. 2016. Alphavirus Infection: Host Cell Shut-Off and Inhibition of Antiviral
701 Responses. *Viruses* **8**:166. doi:10.3390/v8060166
702 Fujii R, Okamoto M, Aratani S, Oishi T, Ohshima T, Taira K, Baba M, Fukamizu A, Nakajima
703 T. 2001. A Role of RNA Helicase A in cis-Acting Transactivation Response Element-
704 mediated Transcriptional Regulation of Human Immunodeficiency Virus Type 1. *J Biol*
705 *Chem* **276**:5445–5451. doi:10.1074/jbc.M006892200
706 Gal-Ben-Ari S, Barrera I, Ehrlich M, Rosenblum K. 2018. PKR: A Kinase to Remember. *Front*
707 *Mol Neurosci* **11**:480. doi:10.3389/fnmol.2018.00480
708 García MA, Meurs EF, Esteban M. 2007. The dsRNA protein kinase PKR: Virus and cell
709 control. *Biochimie* **89**:799–811. doi:10.1016/j.biochi.2007.03.001
710 Girardi E, Chane-Woon-Ming B, Messmer M, Kaukinen P, Pfeffer S. 2013. Identification of
711 RNase L-dependent, 3'-end-modified, viral small RNAs in Sindbis virus-infected
712 mammalian cells. *mBio* **4**:e00698-00613. doi:10.1128/mBio.00698-13
713 Girardi E, Lefèvre M, Chane-Woon-Ming B, Paro S, Claydon B, Imler J-L, Meignin C, Pfeffer
714 S. 2015. Cross-species comparative analysis of Dicer proteins during Sindbis virus
715 infection. *Sci Rep* **5**:10693. doi:10.1038/srep10693
716 Griffin D. 2007. Alphaviruses, p 1023–1067. *Fields Virol 5th Ed Lippincott Williams Wilkins*
717 *Phila PA*.
718 Guo Z, Li Y, Ding S-W. 2019. Small RNA-based antimicrobial immunity. *Nat Rev Immunol*
719 **19**:31–44. doi:10.1038/s41577-018-0071-x
720 Haase AD, Jaskiewicz L, Zhang H, Laine S, Sack R, Gatignol A, Filipowicz W. 2005. TRBP,
721 a regulator of cellular PKR and HIV-1 virus expression, interacts with Dicer and
722 functions in RNA silencing. *EMBO Rep* **6**:961–7.
723 Herbert A, Alfken J, Kim YG, Mian IS, Nishikura K, Rich A. 1997. A Z-DNA binding domain
724 present in the human editing enzyme, double-stranded RNA adenosine deaminase. *Proc*
725 *Natl Acad Sci U S A* **94**:8421–8426. doi:10.1073/pnas.94.16.8421

726 Heyam A, Lagos D, Plevin M. 2015. Dissecting the roles of TRBP and PACT in double-
727 stranded RNA recognition and processing of noncoding RNAs. *WIREs RNA* **6**:271–289.
728 doi:10.1002/wrna.1272
729 Hutvágner G, McLachlan J, Pasquinelli AE, Balint E, Tuschl T, Zamore PD. 2001. A cellular
730 function for the RNA-interference enzyme Dicer in the maturation of the let-7 small
731 temporal RNA. *Science* **293**:834–8.
732 Iizasa H, Wulff B-E, Alla NR, Maragkakis M, Megraw M, Hatzigeorgiou A, Iwakiri D, Takada
733 K, Wiedmer A, Showe L, Lieberman P, Nishikura K. 2010. Editing of Epstein-Barr
734 virus-encoded BART6 microRNAs controls their dicer targeting and consequently
735 affects viral latency. *J Biol Chem* **285**:33358–33370. doi:10.1074/jbc.M110.138362
736 Ivashkiv LB, Donlin LT. 2014. Regulation of type I interferon responses. *Nat Rev Immunol*
737 **14**:36–49. doi:10.1038/nri3581
738 Kennedy EM, Whisnant AW, Kornepati AVR, Marshall JB, Bogerd HP, Cullen BR. 2015.
739 Production of functional small interfering RNAs by an amino-terminal deletion mutant
740 of human Dicer. *Proc Natl Acad Sci* **112**:E6945–E6954. doi:10.1073/pnas.1513421112
741 Kim Y, Lee JH, Park J-E, Cho J, Yi H, Kim VN. 2014. PKR is activated by cellular dsRNAs
742 during mitosis and acts as a mitotic regulator. *Genes Dev* **28**:1310–1322.
743 doi:10.1101/gad.242644.114
744 Kok K-H, Lui P-Y, Ng M-HJ, Siu K-L, Au SWN, Jin D-Y. 2011. The Double-Stranded RNA-
745 Binding Protein PACT Functions as a Cellular Activator of RIG-I to Facilitate Innate
746 Antiviral Response. *Cell Host Microbe* **9**:299–309. doi:10.1016/j.chom.2011.03.007
747 Kok KH, Ng MH, Ching YP, Jin DY. 2007. Human TRBP and PACT Directly Interact with
748 Each Other and Associate with Dicer to Facilitate the Production of Small Interfering
749 RNA. *J Biol Chem* **282**:17649–57.
750 Kuleshov MV, Jones MR, Rouillard AD, Fernandez NF, Duan Q, Wang Z, Koplev S, Jenkins
751 SL, Jagodnik KM, Lachmann A, McDermott MG, Monteiro CD, Gundersen GW,
752 Ma'ayan A. 2016. Enrichr: a comprehensive gene set enrichment analysis web server
753 2016 update. *Nucleic Acids Res* **44**:W90-97. doi:10.1093/nar/gkw377
754 Lambert M, Pépin G, Peralta-Zaragoza O, Matusiak R, Ly S, Landry P, Provost P. 2016.
755 TWEAK Negatively Regulates Human Dicer. *Non-Coding RNA* **2**.
756 doi:10.3390/ncrna2040012
757 Lee Y, Hur I, Park SY, Kim YK, Suh MR, Kim VN. 2006. The role of PACT in the RNA
758 silencing pathway. *Embo J* **25**:522–32.

759 Lemaire PA, Anderson E, Lary J, Cole JL. 2008. Mechanism of PKR Activation by dsRNA. *J*
760 *Mol Biol* **381**:351–360. doi:10.1016/j.jmb.2008.05.056
761 Lepur A, Kovačević L, Belužić R, Vugrek O. 2016. Combining unique multiplex gateway
762 cloning and bimolecular fluorescence complementation (BiFC) for high-throughput
763 screening of protein–protein interactions. *J Biomol Screen* **21**:1100–1111.
764 Li J, Tang H, Mullen TM, Westberg C, Reddy TR, Rose DW, Wong-Staal F. 1999. A role for
765 RNA helicase A in post-transcriptional regulation of HIV type 1. *Proc Natl Acad Sci U*
766 *S A* **96**:709–714. doi:10.1073/pnas.96.2.709
767 Li Y, Basavappa M, Lu J, Dong S, Cronkite DA, Prior JT, Reinecker H-C, Hertzog P, Han Y,
768 Li W-X, Cheloufi S, Karginov FV, Ding S-W, Jeffrey KL. 2016. Induction and
769 suppression of antiviral RNA interference by influenza A virus in mammalian cells. *Nat*
770 *Microbiol* **2**:16250. doi:10.1038/nmicrobiol.2016.250
771 Li Y, Lu J, Han Y, Fan X, Ding S-W. 2013. RNA interference functions as an antiviral
772 immunity mechanism in mammals. *Science* **342**:231–234.
773 doi:10.1126/science.1241911
774 Li Z, Wolff KC, Samuel CE. 2010. RNA adenosine deaminase ADAR1 deficiency leads to
775 increased activation of protein kinase PKR and reduced vesicular stomatitis virus
776 growth following interferon treatment. *Virology* **396**:316–322.
777 doi:10.1016/j.virol.2009.10.026
778 López P, Girardi E, Mounce BC, Weiss A, Chane-Woon-Ming B, Messmer M, Kaukinen P,
779 Kopp A, Bortolamiol-Becet D, Fendri A, Vignuzzi M, Brino L, Pfeffer S. 2020. High-
780 Throughput Fluorescence-Based Screen Identifies the Neuronal MicroRNA miR-124 as
781 a Positive Regulator of Alphavirus Infection. *J Virol* **94**. doi:10.1128/JVI.02145-19
782 Lui P-Y, Wong L-YR, Ho T-H, Au SWN, Chan C-P, Kok K-H, Jin D-Y. 2017. PACT
783 Facilitates RNA-Induced Activation of MDA5 by Promoting MDA5 Oligomerization.
784 *J Immunol* **199**:1846–1855. doi:10.4049/jimmunol.1601493
785 Maillard PV, Ciaudo C, Marchais A, Li Y, Jay F, Ding SW, Voinnet O. 2013. Antiviral RNA
786 interference in mammalian cells. *Science* **342**:235–238. doi:10.1126/science.1241930
787 Maillard PV, van der Veen AG, Poirier EZ, Reis e Sousa C. 2019. Slicing and dicing viruses:
788 antiviral RNA interference in mammals. *EMBO J* **38**. doi:10.15252/embj.2018100941
789 Maillard PV, Veen AGV der, Deddouche-Grass S, Rogers NC, Merits A, Sousa CR e. 2016.
790 Inactivation of the type I interferon pathway reveals long double-stranded RNA-

791 mediated RNA interference in mammalian cells. *EMBO J* **35**:2505–2518.
792 doi:10.15252/embj.201695086
793 Meister G, Tuschl T. 2004. Mechanisms of gene silencing by double-stranded RNA. *Nature*
794 **431**:343–9.
795 Mittelstadt M, Frump A, Khuu T, Fowlkes V, Handy I, Patel CV, Patel RC. 2008. Interaction
796 of human tRNA-dihydrouridine synthase-2 with interferon-induced protein kinase
797 PKR. *Nucleic Acids Res* **36**:998–1008. doi:10.1093/nar/gkm1129
798 Nakamura T, Kunz RC, Zhang C, Kimura T, Yuan CL, Baccaro B, Namiki Y, Gygi SP,
799 Hotamisligil GS. 2015. A Critical Role for PKR Complexes with TRBP in
800 Immunometabolic Regulation and eIF2α Phosphorylation in Obesity. *Cell Rep* **11**:295–
801 307. doi:10.1016/j.celrep.2015.03.021
802 Ota H, Sakurai M, Gupta R, Valente L, Wulff B-E, Ariyoshi K, Iizasa H, Davuluri RV,
803 Nishikura K. 2013. ADAR1 forms a complex with Dicer to promote microRNA
804 processing and RNA-induced gene silencing. *Cell* **153**:575–589.
805 doi:10.1016/j.cell.2013.03.024
806 Parameswaran P, Sklan E, Wilkins C, Burgon T, Samuel MA, Lu R, Ansel KM, Heissmeyer
807 V, Einav S, Jackson W, Doukas T, Paranjape S, Polacek C, dos Santos FB, Jalili R,
808 Babrzadeh F, Gharizadeh B, Grimm D, Kay M, Koike S, Sarnow P, Ronaghi M, Ding
809 SW, Harris E, Chow M, Diamond MS, Kirkegaard K, Glenn JS, Fire AZ. 2010. Six
810 RNA viruses and forty-one hosts: viral small RNAs and modulation of small RNA
811 repertoires in vertebrate and invertebrate systems. *PLoS Pathog* **6**:e1000764.
812 doi:10.1371/journal.ppat.1000764
813 Park H, Davies MV, Langland JO, Chang HW, Nam YS, Tartaglia J, Paoletti E, Jacobs BL,
814 Kaufman RJ, Venkatesan S. 1994. TAR RNA-binding protein is an inhibitor of the
815 interferon-induced protein kinase PKR. *Proc Natl Acad Sci U S A* **91**:4713–4717.
816 doi:10.1073/pnas.91.11.4713
817 Patel CV, Handy I, Goldsmith T, Patel RC. 2000. PACT, a Stress-modulated Cellular Activator
818 of Interferon-induced Double-stranded RNA-activated Protein Kinase, PKR. *J Biol*
819 *Chem* **275**:37993–37998. doi:10.1074/jbc.M004762200
820 Perez-Riverol Y, Csordas A, Bai J, Bernal-Llinares M, Hewapathirana S, Kundu DJ, Inuganti
821 A, Griss J, Mayer G, Eisenacher M, Pérez E, Uszkoreit J, Pfeuffer J, Sachsenberg T,
822 Yilmaz S, Tiwary S, Cox J, Audain E, Walzer M, Jarnuczak AF, Ternent T, Brazma A,
823 Vizcaíno JA. 2019. The PRIDE database and related tools and resources in 2019:

824 improving support for quantification data. *Nucleic Acids Res* **47**:D442–D450.
825 doi:10.1093/nar/gky1106
826 Pfaller CK, Li Z, George CX, Samuel CE. 2011. Protein kinase PKR and RNA adenosine
827 deaminase ADAR1: new roles for old players as modulators of the interferon response.
828 *Curr Opin Immunol*, Special section: Cytokines/Immunogenetics and transplantation
829 **23**:573–582. doi:10.1016/j.coi.2011.08.009
830 Qiu Y, Xu Y, Zhang Y, Zhou H, Deng Y-Q, Li X-F, Miao M, Zhang Q, Zhong B, Hu Y, Zhang
831 F-C, Wu L, Qin C-F, Zhou X. 2017. Human Virus-Derived Small RNAs Can Confer
832 Antiviral Immunity in Mammals. *Immunity* **46**:992-1004.e5.
833 doi:10.1016/j.immuni.2017.05.006
834 Qiu Y, Xu Y-P, Wang M, Miao M, Zhou H, Xu J, Kong J, Zheng D, Li R-T, Zhang R-R. 2020.
835 Flavivirus induces and antagonizes antiviral RNA interference in both mammals and
836 mosquitoes. *Sci Adv* **6**:eaax7989.
837 Robb GB, Rana TM. 2007. RNA helicase A interacts with RISC in human cells and functions
838 in RISC loading. *Mol Cell* **26**:523–537. doi:10.1016/j.molcel.2007.04.016
839 Roy BB, Hu J, Guo X, Russell RS, Guo F, Kleiman L, Liang C. 2006. Association of RNA
840 helicase a with human immunodeficiency virus type 1 particles. *J Biol Chem*
841 **281**:12625–12635. doi:10.1074/jbc.M510596200
842 Ryman KD, White LJ, Johnston RE, Klimstra WB. 2002. Effects of PKR/RNase L-Dependent
843 and Alternative Antiviral Pathways on Alphavirus Replication and Pathogenesis. *Viral*
844 *Immunol* **15**:53–76. doi:10.1089/088282402317340233
845 Sadler AJ, Latchoumanin O, Hawkes D, Mak J, Williams BRG. 2009. An Antiviral Response
846 Directed by PKR Phosphorylation of the RNA Helicase A. *PLoS Pathog* **5**:e1000311.
847 doi:10.1371/journal.ppat.1000311
848 Samuel CE. 2011. Adenosine deaminases acting on RNA (ADARs) are both antiviral and
849 proviral. *Virology* **411**:180–193. doi:10.1016/j.virol.2010.12.004
850 Schoggins JW, Wilson SJ, Panis M, Murphy MY, Jones CT, Bieniasz P, Rice CM. 2011. A
851 diverse range of gene products are effectors of the type I interferon antiviral response.
852 *Nature* **472**:481–485. doi:10.1038/nature09907
853 Schuster S, Overheul GJ, Bauer L, van Kuppeveld FJM, van Rij RP. 2019. No evidence for
854 viral small RNA production and antiviral function of Argonaute 2 in human cells. *Sci*
855 *Rep* **9**:1–11. doi:10.1038/s41598-019-50287-w

856 Singh M, Castillo D, Patel CV, Patel RC. 2011. Stress-induced phosphorylation of PACT
857 reduces its interaction with TRBP and leads to PKR activation. *Biochemistry* **50**:4550–
858 4560. doi:10.1021/bi200104h
859 Takahashi T, Nakano Y, Onomoto K, Murakami F, Komori C, Suzuki Y, Yoneyama M, Ui-Tei
860 K. 2018a. LGP2 virus sensor regulates gene expression network mediated by TRBP-
861 bound microRNAs. *Nucleic Acids Res* **46**:9134–9147. doi:10.1093/nar/gky575
862 Takahashi T, Nakano Y, Onomoto K, Yoneyama M, Ui-Tei K. 2018b. Virus Sensor RIG-I
863 Represses RNA Interference by Interacting with TRBP through LGP2 in Mammalian
864 Cells. *Genes* **9**:511. doi:10.3390/genes9100511
865 Takahashi T, Ui-Tei K. 2020. Mutual Regulation of RNA Silencing and the IFN Response as
866 an Antiviral Defense System in Mammalian Cells. *Int J Mol Sci* **21**:1348.
867 doi:10.3390/ijms21041348
868 tenOever BR. 2016. The Evolution of Antiviral Defense Systems. *Cell Host Microbe* **19**:142–
869 149. doi:10.1016/j.chom.2016.01.006
870 Tsai K, Courtney DG, Kennedy EM, Cullen BR. 2018. Influenza A virus-derived siRNAs
871 increase in the absence of NS1 yet fail to inhibit virus replication. *RNA N Y N*.
872 doi:10.1261/rna.066332.118
873 van der Veen AG, Maillard PV, Schmidt JM, Lee SA, Deddouche-Grass S, Borg A, Kjær S,
874 Snijders AP, Reis e Sousa C. 2018. The RIG-I-like receptor LGP2 inhibits Dicer-
875 dependent processing of long double-stranded RNA and blocks RNA interference in
876 mammalian cells. *EMBO J* **37**:e97479. doi:10.15252/embj.201797479
877 Wienholds E, Koudijs MJ, Van Eeden FJ, Cuppen E, Plasterk RH. 2003. The microRNA-
878 producing enzyme Dicer1 is essential for zebrafish development. *Nat Genet* 217–218.
879 Williams BR. 1999. PKR; a sentinel kinase for cellular stress. *Oncogene* **18**:6112–6120.
880 doi:10.1038/sj.onc.1203127
881 Yang W, Chendrimada TP, Wang Q, Higuchi M, Seeburg PH, Shiekhattar R, Nishikura K.
882 2006. Modulation of microRNA processing and expression through RNA editing by
883 ADAR deaminases. *Nat Struct Mol Biol* **13**:13–21.
884
885

886 ## Figure legends

887 **Figure 1: Molecular characterization of FHA:DICER cell line.**

888 **A,** Western blot analysis of DICER (DICER and HA), TRBP and AGO2 expression in HEK
889 293T, NoDice and FHA:DICER cell lines. Alpha-Tubulin was used as loading control. **B,** miR-
890 16 expression analyzed by northern blot in the same samples as in A**.** Expression of snRNA U6
891 was used as loading control. **C,** GFP fluorescent microscopy pictures of HEK 293T, NoDice
892 and FHA:DICER cell lines infected with SINV-GFP at an MOI of 0.02 for 24 h. The left panel
893 corresponds to GFP signal from infected cells and the right panel to a merge picture of GFP
894 signal and brightfield. Pictures were taken with a 5x magnification. hpi: hours post-infection.
895 **D,** Representative western blot of DICER (DICER and HA) and GFP expression in SINV-GFP-
896 infected cells in the same condition as in C. Alpha-Tubulin was used as loading control. **E**,
897 Mean (+/- SEM) of SINV-GFP viral titers in HEK 293T, NoDice and FHA:DICER cells
898 infected at an MOI of 0.02 for 24 h (n = 3) from plaque assay quantification. * $p < 0.05$, ** $p <$
899 0.005, ordinary one-way ANOVA test.

900

901 **Figure 2: LC-MS/MS analysis of DICER interactome during SINV infection.**

902 **A,** Volcano plot for differentially expressed proteins (DEPs) between HA IP and CTL IP in
903 FHA:DICER mock-infected cells. Each protein is marked as a dot; proteins that are
904 significantly up-regulated in HA IP are shown in red, up-regulated proteins in CTL IP are
905 shown in blue, and non-significant proteins are in black. The horizontal line denotes the
906 adjusted p-value threshold (0.05) and the vertical lines the Log2 fold change cutoff (-1 and 1).
907 DICER and its cofactors (TRBP, PACT, AGO2) are highlighted in yellow. **B,** Left panel:
908 Volcano plot for DEPs between SINV-GFP (MOI of 2, 6 hpi) and mock fractions of HA IP in
909 FHA:DICER cells. Same colour code and thresholds as in A have been applied. Proteins that
910 are discussed in the text are highlighted in yellow and SINV proteins in purple. **C,** Gene

911 Ontology (GO) term enrichment of proteins up-regulated in SINV-GFP fraction of HA IP using
912 Enrichr software (Chen et al., 2013; Kuleshov et al., 2016). The graph displays the GO term
913 hierarchy within the "biological process" branch sorted by p-value ranking computed from the
914 Fisher exact test. The length of each bar represents the significance of that specific term. In
915 addition, the brighter the colour is, the more significant that term is. Viral proteins have been
916 excluded for this analysis. **D,** Summary of the differential expression analysis of SINV-GFP vs
917 mock fractions from HA IP in FHA:DICER cells. The analysis has been performed using a
918 generalized linear model of a negative-binomial distribution and p-values were corrected for
919 multiple testing using the Benjamini-Hochberg method.
920
921 **Figure 3: Confirmation of LC-MS/MS analysis by co-IP and BiFC.**
922 **A,** Western blot analysis of HA co-IP in mock or SINV-GFP-infected (MOI of 2, 6 hpi)
923 FHA:DICER cells. Proteins associated to FHA:DICER were revealed by using antibodies
924 targeting endogenous ADAR-1, PKR, TRBP, DHX9 or PACT proteins. In parallel, an HA
925 antibody was used to verify the IP efficiency and GFP antibody was used to verify the infection.
926 Ponceau was used as loading control. **B,** Western blot analysis to validate the interaction of
927 PKR with PACT (upper panel) and DICER (lower panel) in mock or SINV-GFP-infected HEK
928 293T cells. Immunoprecipitated proteins obtained from PKR pulldowns were compared to IgG
929 pulldowns to verify the specificity of the assay. **C,** Interactions between DICER and TRBP,
930 PKR or PACT was visualized by BiFC. Plasmids expressing $^{N\text{-}ter}$Venus:DICER and TRBP:,
931 PACT: or PKR:Venus$^{C\text{-}ter}$ were co-transfected in NoDice/ΔPKR cells for 24 h and cells were
932 either infected with SINV at an MOI of 2 for 6 h or not. The different combinations are indicated
933 on the left side. Reconstitution of Venus (BiFC) signal was observed under epifluorescence
934 microscope. For each condition, the left panel corresponds to Venus signal and the right panel
935 to the corresponding brightfield pictures. Scale bar: 100 μm. **D,** BiFC experiment on fixed

936 NoDice/ΔPKR cells treated as in C. After fixation, cells were stained with DAPI and observed
937 under confocal microscope. Only a merge picture of BiFC and DAPI signals of SINV-infected
938 cells is shown here. A higher magnification of picture showing cytoplasmic localization of the
939 interaction represented by a red square is shown in the bottom left corner. Scale bar: 20 μm and
940 10 μm.
941
942 **Figure 4: Identification of DICER domains involved in DICER-PKR interaction.**
943 **A,** Schematic representation of Human DICER proteins used in this study. The different
944 conserved domains are shown in colored boxes. DUF283: Domain of Unknown Function; PAZ:
945 PIWI ARGONAUTE ZWILLE domain; dsRBD: dsRNA-binding domain. hDICER WT is the
946 full-length protein. hDICER N1 is deleted of the first N-terminal 495 amino acids. hDICER N3
947 is wholly deleted of the helicase domain. hDICER Hel. is the whole DICER's helicase domain.
948 hDICER ΔdsRBD is deleted of the C-terminal dsRBD. **B,** Western blot analysis of HA co-IP
949 in NoDice cells transfected with different versions of FHA:DICER proteins and infected with
950 SINV-GFP (MOI of 2, 6 hpi). Efficiency of immunoprecipitation was assessed using an anti-
951 Flag antibody and co-IPs of PKR, TRBP, PACT and p-PKR were examined using appropriate
952 antibodies. Expression of GFP in INPUT fraction was visualized as control of SINV-GFP
953 infection. Ponceau staining of membranes is used as loading control. **C,** Plasmids expressing
954 the different versions of DICER proteins fused to the N-terminal part of Venus and
955 PKR:Venus$^{C\text{-}ter}$ plasmid were co-transfected in NoDice/ΔPKR cells. Cells were treated as in Fig
956 3C. The different combinations are noted on the left side. The fluorescent signal was observed
957 using an epifluorescence microscope. For each condition, the left panel corresponds to Venus
958 signal and the right panel to the corresponding brightfield pictures. Scale bar: 100 μm.
959
960 **Figure 5: Analysis of SINV-GFP infection in FHA:DICER N1 cell line.**

961 **A,** Expression of DICER (DICER, HA), TRBP and AGO2 was analysed by western blot in
962 HEK 293T, NoDice, FHA:DICER and FHA:DICER N1 cell lines. Alpha-Tubulin was used as
963 loading control. **B,** Northern blot analysis of miR-16 expression in the same samples as in A.
964 Expression of snRNA U6 was used as loading control. **C,** Representative GFP fluorescent
965 microscopy images of HEK 293T, NoDice, FHA:DICER and FHA:DICER N1 cell lines
966 infected with SINV-GFP at an MOI of 0.02 for 24 h. The left panel corresponds to GFP signal
967 and the right panel to a merge picture of GFP signal and brightfield. Pictures were taken with a
968 5x magnification. hpi: hours post-infection. **D,** Western blot analysis of DICER (DICER and
969 HA) and GFP expression in SINV-GFP-infected cells in the same condition as in C. alpha-
970 Tubulin was used as loading control. **E**, Mean (+/- SEM) of SINV-GFP viral titers fold change
971 over HEK 293T cells in HEK 293T, NoDice, FHA:DICER and FHA:DICER N1 cell lines
972 infected at an MOI of 0.02 for 24 h (n = 3) from plaque assay quantification. * $p < 0.05$, ** $p <$
973 0.01, ordinary one-way ANOVA test.
974

975 # Supplementary material

976

977 **Supplementary figures legends**

978 **Figure S1: Analysis of SINV-GFP infection in FHA:DICER cell line at different MOI and**
979 **time points.**

980 HEK 293T, NoDice and FHA:DICER cells were infected with SINV-GFP at an MOI of 2 for
981 16 h (**A**) or 6 h (**B**). Upper panel: Representative GFP pictures of infected cells. The left panel
982 corresponds to GFP signal and the right panel to a merge of GFP signal and the corresponding
983 brightfield. Pictures were taken with a 5x magnification. hpi: hours post-infection. Middle
984 panel: Western blot analysis of DICER (DICER and HA) and GFP expression in SINV-GFP-
985 infected cells. Alpha-Tubulin was used as loading control. Bottom panel: Mean (+/- SEM) of
986 SINV-GFP viral titers in HEK 293T, NoDice and FHA:DICER cells infected at an MOI of 2
987 for 16 h (left panel n = 4) or for 6 h (right panel n = 3) from plaque assay quantification. * $p <$
988 0.05, *** $p < 0.001$, ns non-significant. ordinary one-way ANOVA test.

989

990 **Figure S2: LC-MS/MS analysis of DICER interactome during SFV infection.**

991 **A,** Volcano plot for differentially expressed proteins (DEPs) between HA IP and CTL IP in
992 FHA:DICER mock-infected cells. Each protein is marked as a dot; proteins that are
993 significantly up-regulated in HA IP are shown in red, up-regulated proteins in CTL IP are
994 shown in blue, and non-significant proteins are in black. The horizontal line denotes the
995 adjusted p-value threshold (0.05) and the vertical lines the Log2 fold change cutoff (-1 and 1).
996 DICER and its cofactors (TRBP, PACT, AGO2) are highlighted in yellow. **B,** Left panel:
997 Volcano plot for DEPs between SFV (MOI of 2, 6 hpi) and mock fractions of HA IP in
998 FHA:DICER cells. Same colour code and thresholds as in A were applied. Proteins that are
999 discussed in the text are highlighted in yellow and SFV proteins in purple. **C,** Summary of the

1000 differential expression analysis of SFV vs mock fractions from HA IP in FHA:DICER cells.
1001 The analysis has been performed using a generalized linear model of a negative-binomial
1002 distribution and p-values were corrected for multiple testing using the Benjamini-Hochberg
1003 method.
1004
1005 **Figure S3: Confirmation of LC-MS/MS analysis by co-IP and BiFC controls.**
1006 **A,** FHA:DICER cells were infected with SINV-GFP at an MOI of 0.02 for 24 h and a HA co-
1007 IP was performed. Eluted proteins were resolved by western blot and IP efficiency was assessed
1008 using an HA antibody. In parallel, co-IPed proteins were visualized using appropriate
1009 antibodies. GFP antibody was used to verify the infection and Ponceau staining serves as
1010 loading control. **B,** Schematic representation of Human DICER proteins used for BiFC positive
1011 and negative controls. The different conserved domains are shown in colored boxes. DUF283:
1012 Domain of Unknown Function; PAZ: PIWI ARGONAUTE ZWILLE domain; dsRBD:
1013 dsRNA-binding domain. hDICER WT is the full-length protein. hDICER N1 is deleted of the
1014 first N-terminal 495 amino acids. **C,** In parallel to BiFC assay, expression of BiFC plasmids
1015 was assessed by western blot. DICER proteins (WT and N1) and PKR were visualized using
1016 antibodies targeting endogenous proteins, whereas TRBP and PACT were detected using GFP
1017 antibody. Antibody targeting the SINV coat protein (CP) was used as infection control. Ponceau
1018 staining was used as loading control. **D,** Positive and negative BiFC controls on fixed
1019 NoDice/ΔPKR cells. After co-transfection, cells were infected with SINV at an MOI of 2 for 6
1020 h and fixed. After fixation, cells were stained with DAPI and observed under confocal
1021 microscope. Merge pictures of BiFC and DAPI signals of SINV-infected cells are shown. A
1022 higher magnification of images showing the interaction represented by a red square is shown
1023 in the bottom left corner. Scale bar: 20 μm and 10 μm.
1024

1025 **Figure S4: Interaction analysis between the different versions of DICER and TRBP or**
1026 **PACT using BiFC assay.**
1027 NoDice/ΔPKR cells were co-transfected for 24 h with plasmids expressing the different
1028 versions of DICER proteins fused to the N-terminal part of Venus and either TRBP:Venus$^{C\text{-}ter}$
1029 (**A**) or PACT:Venus$^{C\text{-}ter}$ (**B**). Cells were then infected with SINV at an MOI of 2 for 6 h and
1030 Venus signal was observed under epifluorescence microscope. The left panel corresponds to
1031 Venus signal and the right panel to the corresponding brightfield picture. Pictures were taken
1032 with a 5x magnification. hpi: hours post-infection. Scale bar: 100 µm.
1033
1034 **Supplementary tables**
1035 **Supp. Table 1:** Top 100 proteins that are differentially immunoprecipitated in Mock infected
1036 FHA:DICER cells by the HA and Myc (CTL) antibodies. Related to Figure 2.
1037
1038 **Supp. Table 2:** Top 100 proteins that are differentially immunoprecipitated with the HA
1039 antibody in SINV-infected vs. Mock-infected FHA:DICER cells. Related to Figure 2.
1040
1041 **Supp. Table 3:** Top 100 proteins that are differentially immunoprecipitated in Mock infected
1042 FHA:DICER cells by the HA and Myc (CTL) antibodies, in the SFV infection experiment.
1043 Related to Figure S2.
1044
1045 **Supp. Table 4:** Top 100 proteins that are differentially immunoprecipitated with the HA
1046 antibody in SFV-infected vs. Mock-infected FHA:DICER cells. Related to Figure S2.
1047
1048 **Supp. Table 5:** List of primers used in this study.

Figure 1

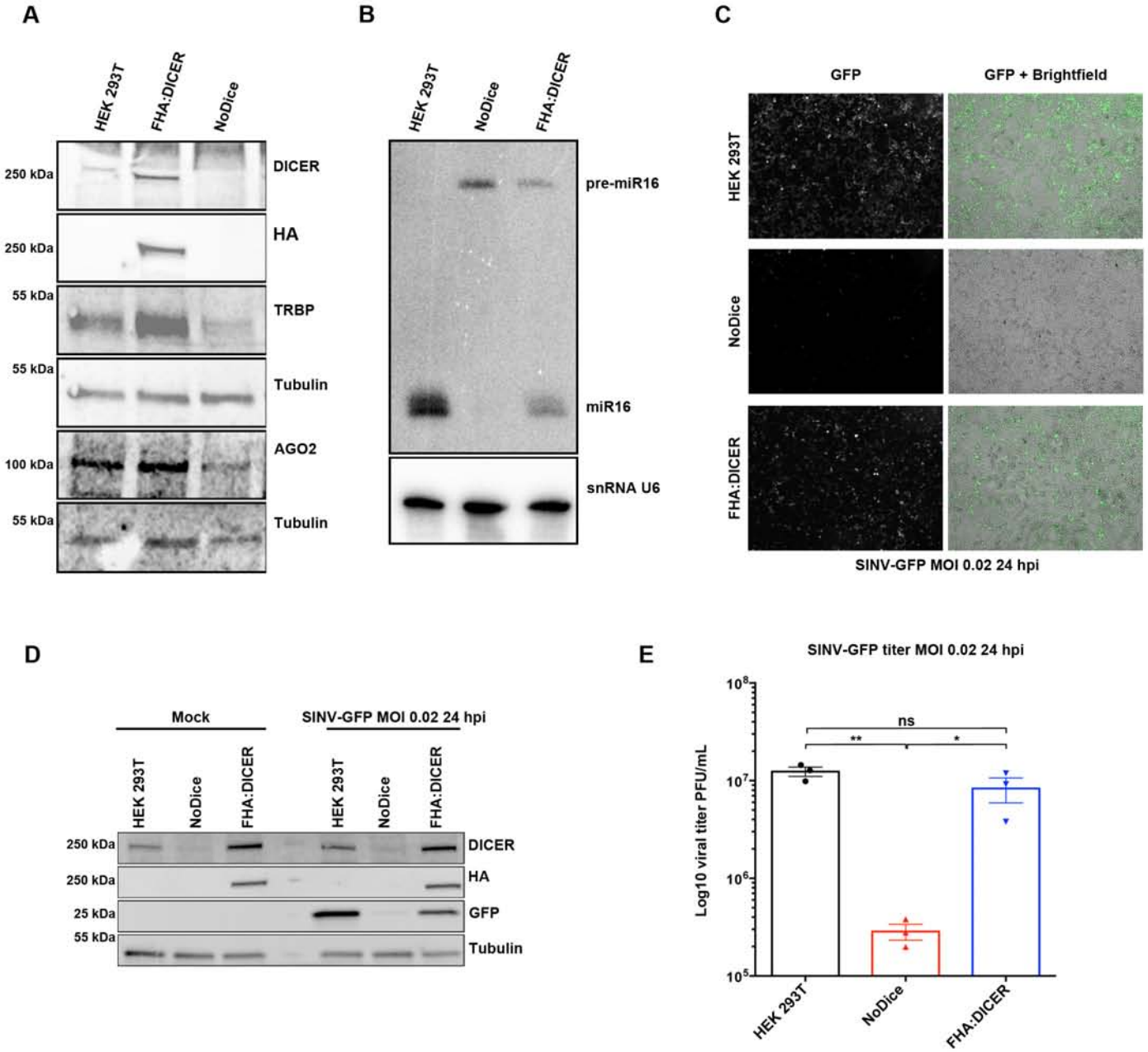
A
HEK 293T
FHA:DICER
NoDice
250 kDa
DICER
250 kDa
HA
55 kDa
TRBP
55 kDa
Tubulin
100 kDa
AGO2
55 kDa
Tubulin
B
HEK 293T
NoDice
FHA:DICER
pre-miR16
miR16
snRNA U6
C
GFP
GFP + Brightfield
HEK 293T
NoDice
FHA:DICER
SINV-GFP MOI 0.02 24 hpi
D
Mock
SINV-GFP MOI 0.02 24 hpi
HEK 293T
NoDice
FHA:DICER
HEK 293T
NoDice
FHA:DICER
250 kDa
DICER
250 kDa
HA
25 kDa
GFP
55 kDa
Tubulin
E
SINV-GFP titer MOI 0.02 24 hpi
Log10 viral titer PFU/mL
ns
**
*
HEK 293T
NoDice
FHA:DICER

Figure 2

A

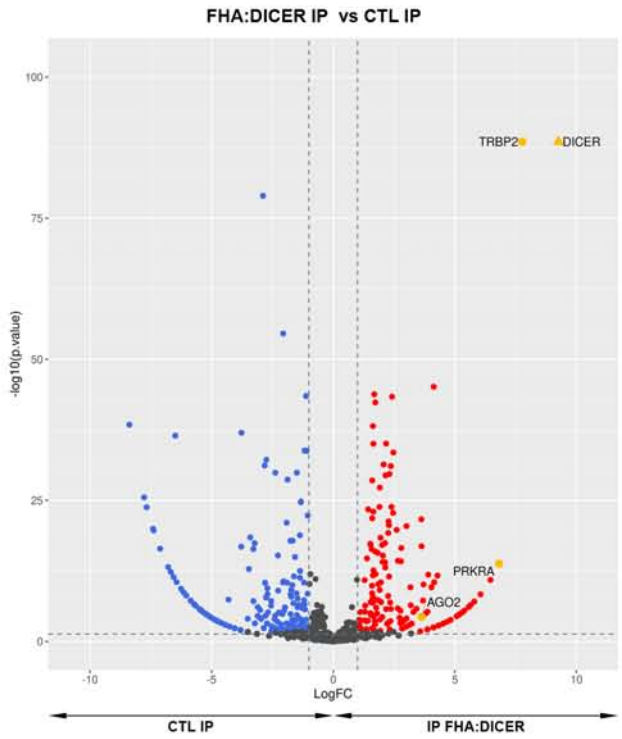

B

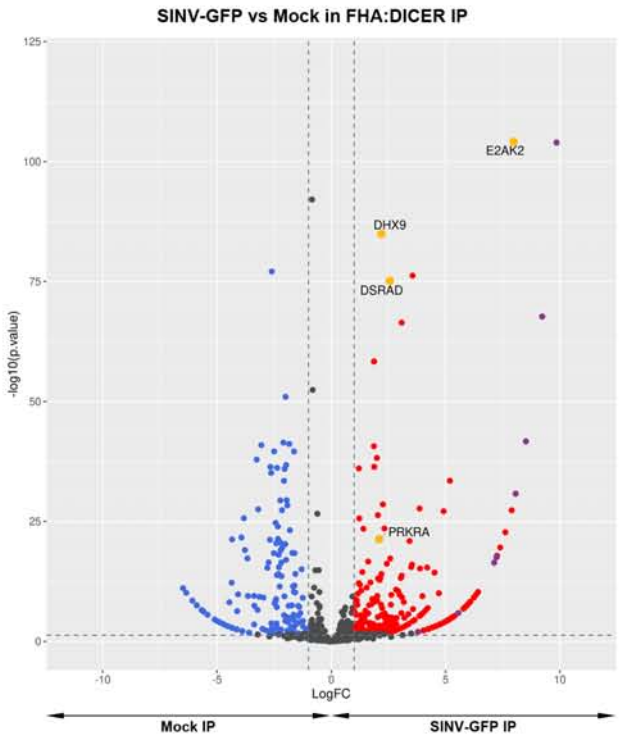

C

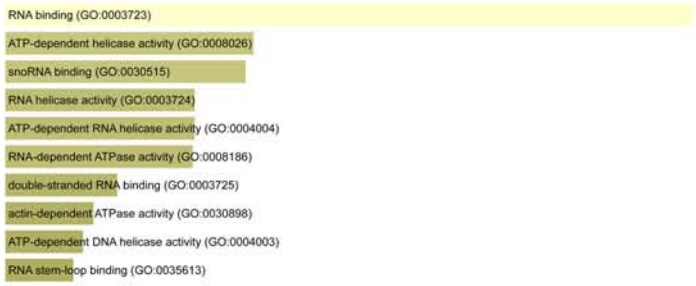

D

Gene name	Mean spectral count		LogFC	Adjusted p-value
	SINV-GFP IP	MOCK IP		
E2AK2 (PKR)	123.3	0.3	7.979	7.316e-102
DSRAD (ADAR-1)	181.3	28.3	2.563	1.421e-73
DHX9	247.3	50	2.194	4.012e-83
PRKRA (PACT)	63.3	13.7	2.093	1.158e-20

Figure 3

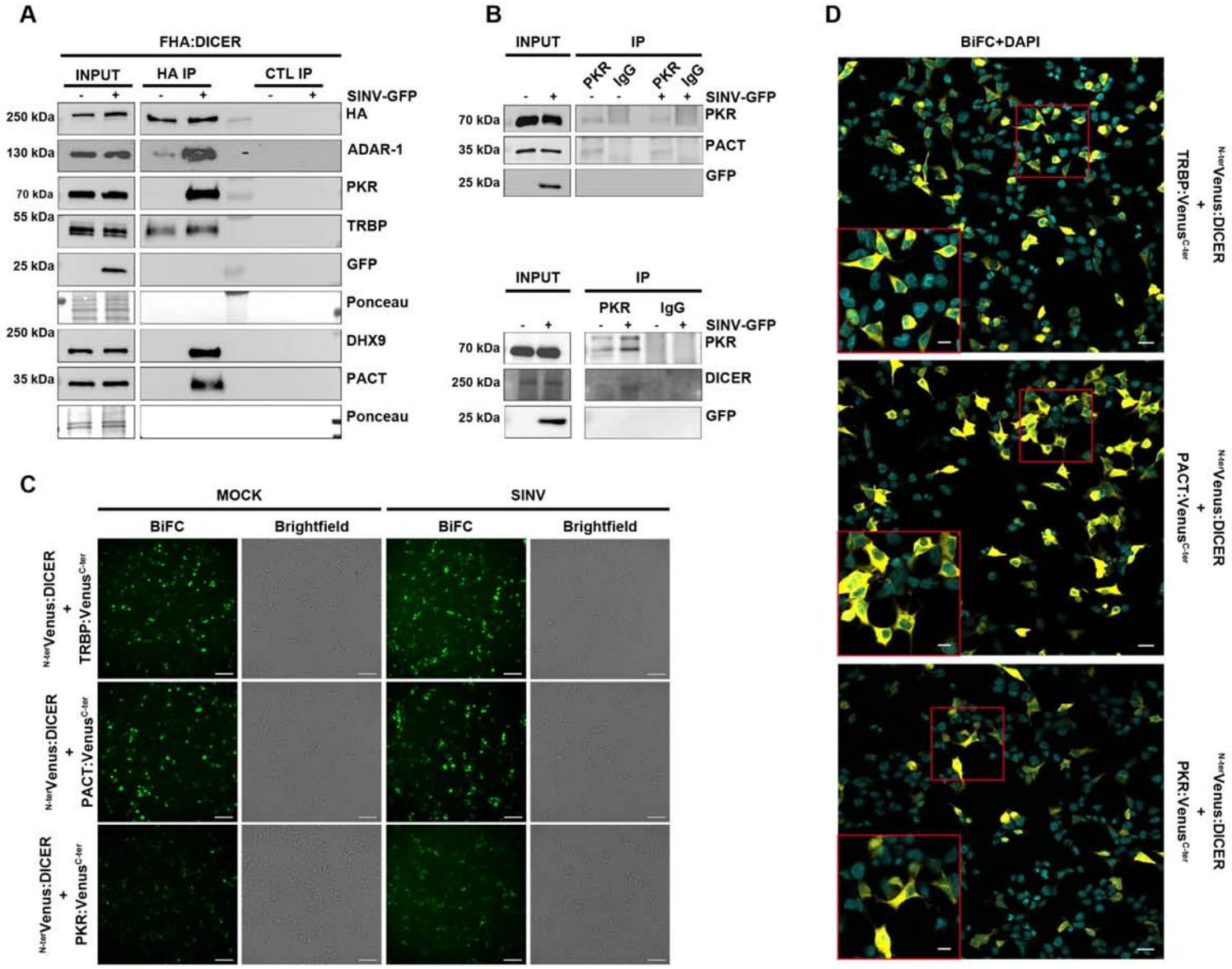
A
FHA:DICER
INPUT
HA IP
CTL IP
SINV-GFP
250 kDa
HA
130 kDa
ADAR-1
70 kDa
PKR
55 kDa
TRBP
25 kDa
GFP
Ponceau
250 kDa
DHX9
35 kDa
PACT
Ponceau
B
INPUT
IP
PKR
IgG
PKR
IgG
SINV-GFP
70 kDa
PKR
35 kDa
PACT
25 kDa
GFP
INPUT
IP
PKR
IgG
SINV-GFP
70 kDa
PKR
250 kDa
DICER
25 kDa
GFP
C
MOCK
SINV
BiFC
Brightfield
BiFC
Brightfield
N-terVenus:DICER + TRBP:VenusC-ter
N-terVenus:DICER + PACT:VenusC-ter
N-terVenus:DICER + PKR:VenusC-ter
D
BiFC+DAPI
N-terVenus:DICER + TRBP:VenusC-ter
N-terVenus:DICER + PACT:VenusC-ter
N-terVenus:DICER + PKR:VenusC-ter

Figure 4

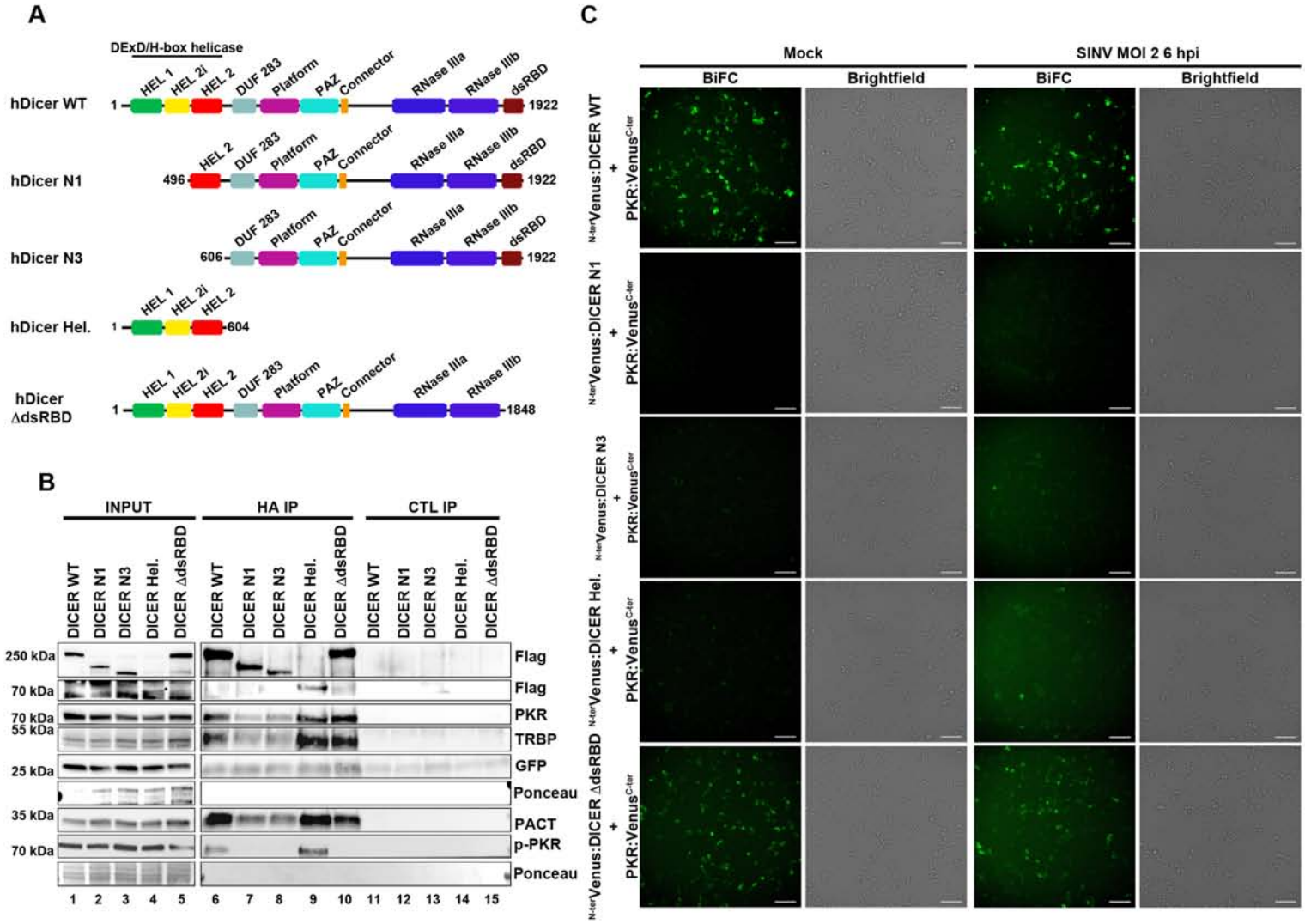
A
DExD/H-box helicase
HEL 1
HEL 2i
HEL 2
DUF 283
Platform
PAZ
Connector
RNase IIIa
RNase IIIb
dsRBD
hDicer WT
1
1922
hDicer N1
496
hDicer N3
606
hDicer Hel.
604
hDicer ΔdsRBD
1848
B
INPUT
HA IP
CTL IP
DICER WT
DICER N1
DICER N3
DICER Hel.
DICER ΔdsRBD
250 kDa
70 kDa
55 kDa
25 kDa
35 kDa
Flag
PKR
TRBP
GFP
Ponceau
PACT
p-PKR
1 2 3 4 5 6 7 8 9 10 11 12 13 14 15
C
Mock
SINV MOI 2 6 hpi
BiFC
Brightfield
N-terVenus:DICER WT
N-terVenus:DICER N1
N-terVenus:DICER N3
N-terVenus:DICER Hel.
N-terVenus:DICER ΔdsRBD
PKR:VenusC-ter

Figure 5

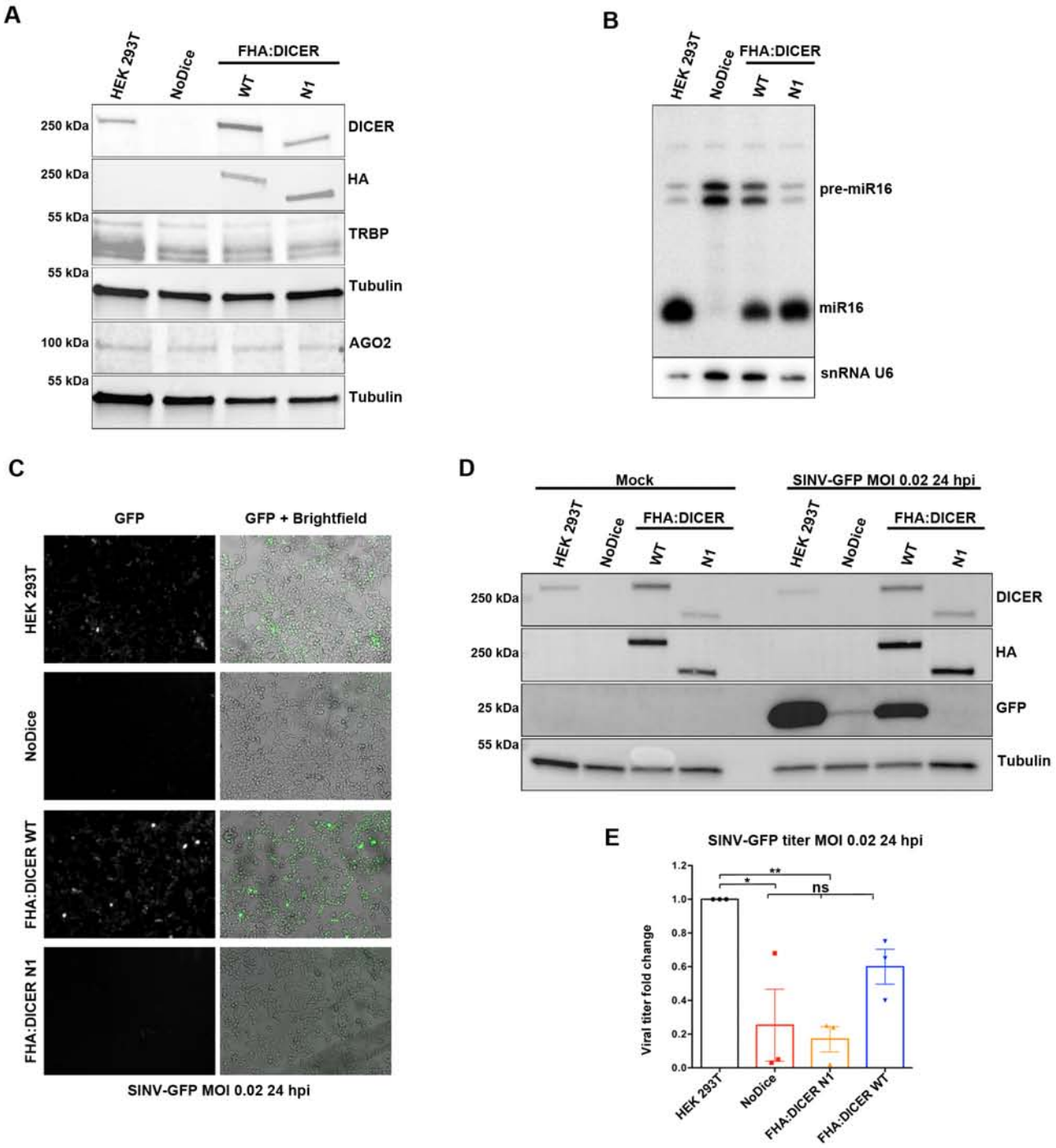
A
HEK 293T
NoDice
FHA:DICER
WT
N1
250 kDa
DICER
250 kDa
HA
55 kDa
TRBP
55 kDa
Tubulin
100 kDa
AGO2
55 kDa
Tubulin
B
HEK 293T
NoDice
FHA:DICER
WT
N1
pre-miR16
miR16
snRNA U6
C
GFP
GFP + Brightfield
HEK 293T
NoDice
FHA:DICER WT
FHA:DICER N1
SINV-GFP MOI 0.02 24 hpi
D
Mock
SINV-GFP MOI 0.02 24 hpi
HEK 293T
NoDice
FHA:DICER
WT
N1
250 kDa
DICER
250 kDa
HA
25 kDa
GFP
55 kDa
Tubulin
E
SINV-GFP titer MOI 0.02 24 hpi
Viral titer fold change
1.2
1.0
0.8
0.6
0.4
0.2
0.0
**
*
ns
HEK 293T
NoDice
FHA:DICER N1
FHA:DICER WT

Figure S1

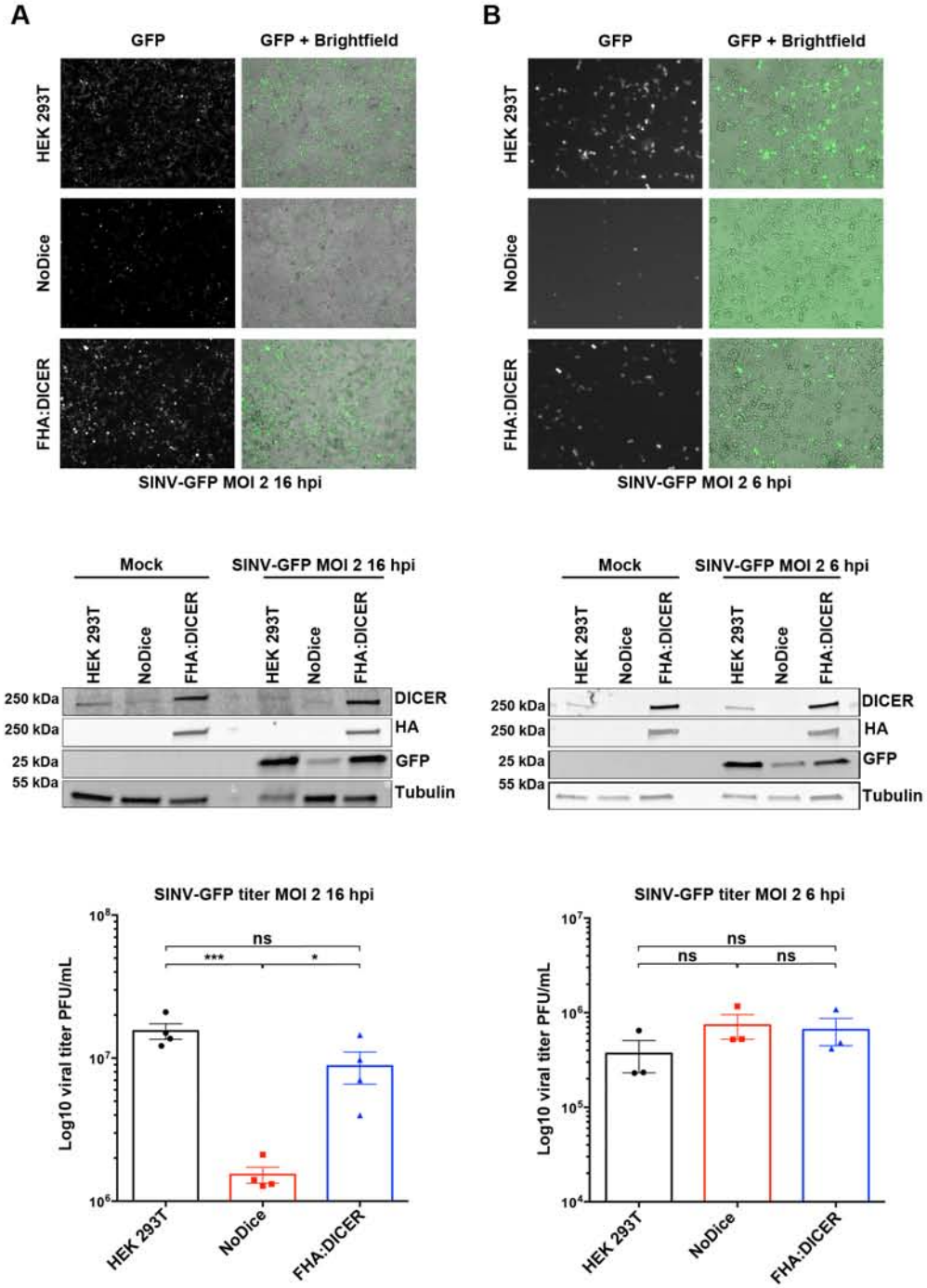
A
GFP
GFP + Brightfield
HEK 293T
NoDice
FHA:DICER
SINV-GFP MOI 2 16 hpi
B
GFP
GFP + Brightfield
HEK 293T
NoDice
FHA:DICER
SINV-GFP MOI 2 6 hpi
Mock
SINV-GFP MOI 2 16 hpi
HEK 293T
NoDice
FHA:DICER
HEK 293T
NoDice
FHA:DICER
250 kDa
250 kDa
25 kDa
55 kDa
DICER
HA
GFP
Tubulin
Mock
SINV-GFP MOI 2 6 hpi
HEK 293T
NoDice
FHA:DICER
HEK 293T
NoDice
FHA:DICER
250 kDa
250 kDa
25 kDa
55 kDa
DICER
HA
GFP
Tubulin
SINV-GFP titer MOI 2 16 hpi
Log10 viral titer PFU/mL
ns
***
*
HEK 293T
NoDice
FHA:DICER
SINV-GFP titer MOI 2 6 hpi
Log10 viral titer PFU/mL
ns
ns
ns
HEK 293T
NoDice
FHA:DICER

Figure S2

A

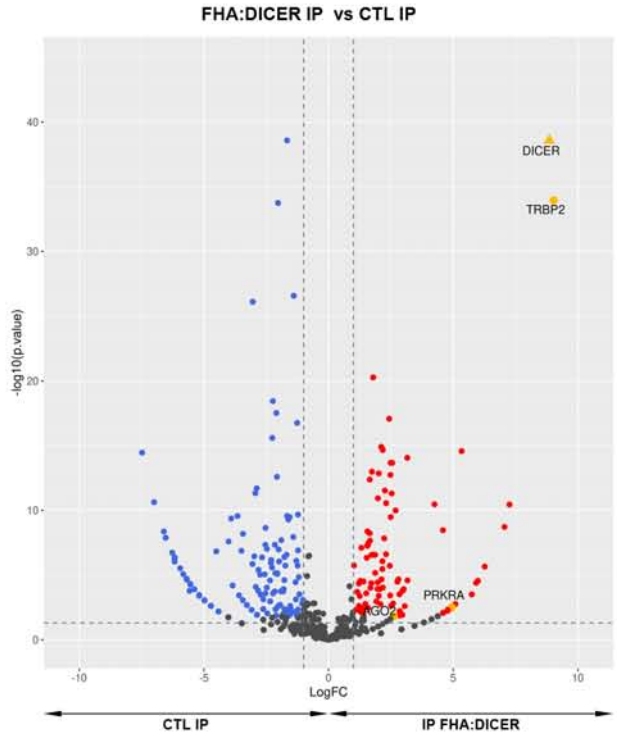

B

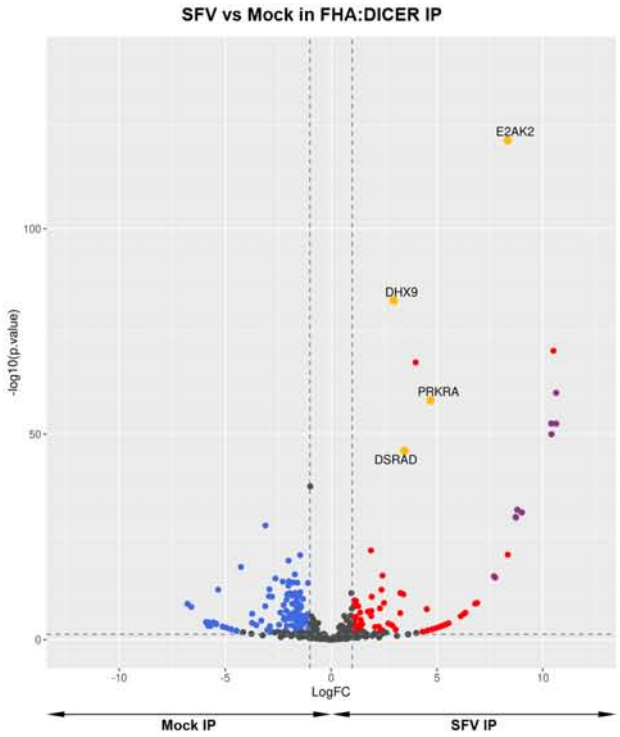

C

Gene name	Mean spectral count		LogFC	Adjusted p-value
	SFV IP	Mock IP		
E2AK2 (PKR)	221	0.5	8.344	2.611e-119
PRKRA (PACT)	131.5	4.5	4.697	8.415e-57
DSRAD (ADAR-1)	268	22	3.466	9.118e-45
DHX9	265	31	2.955	1.245e-80

Figure S3

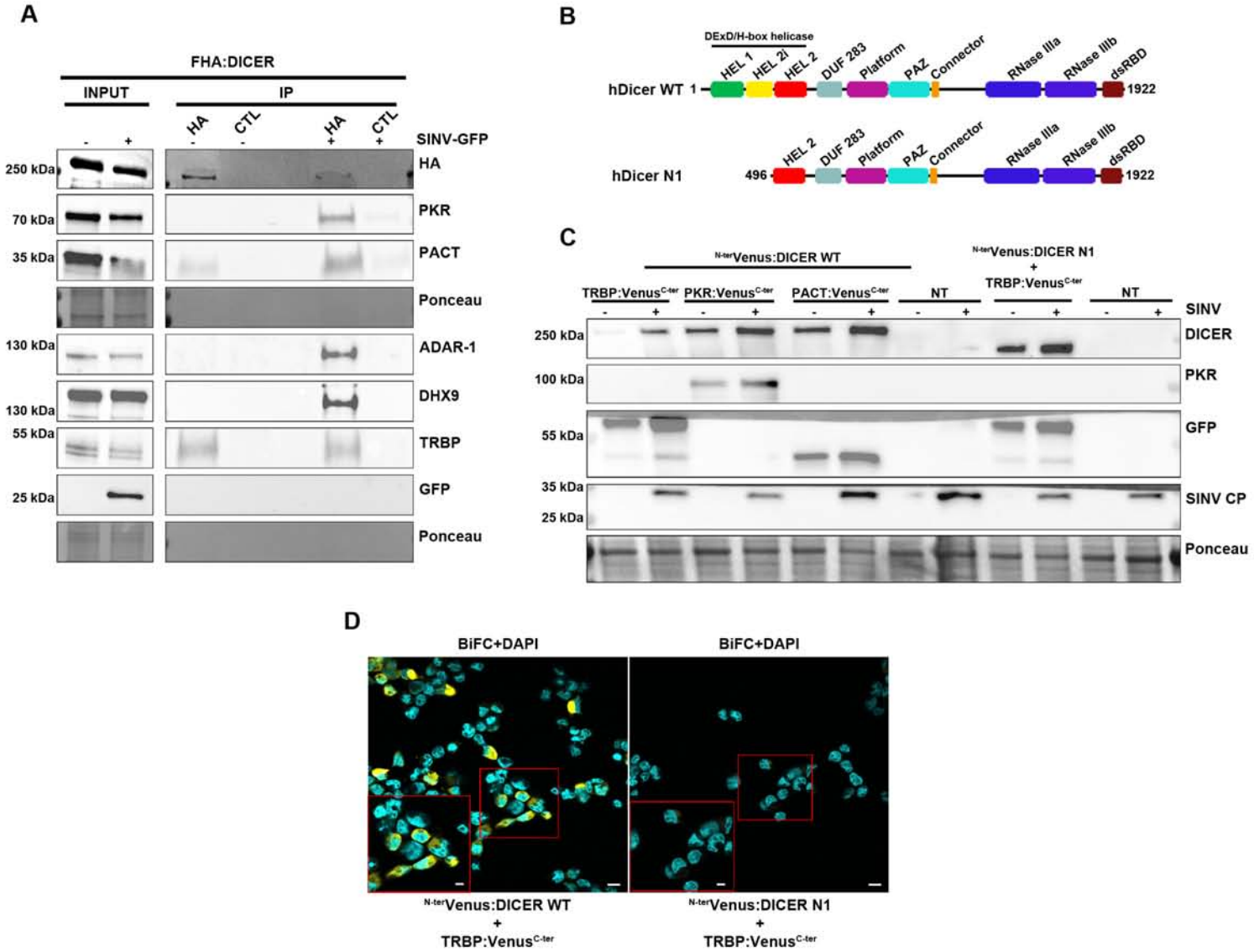
A
FHA:DICER
INPUT
IP
HA
CTL
HA
CTL
SINV-GFP
250 kDa
HA
70 kDa
PKR
35 kDa
PACT
Ponceau
130 kDa
ADAR-1
130 kDa
DHX9
55 kDa
TRBP
25 kDa
GFP
Ponceau
B
DExD/H-box helicase
HEL 1
HEL 2i
HEL 2
DUF 283
Platform
PAZ
Connector
RNase IIIa
RNase IIIb
dsRBD
hDicer WT 1
1922
hDicer N1
496
1922
C
N-terVenus:DICER WT
N-terVenus:DICER N1
+
TRBP:VenusC-ter
TRBP:VenusC-ter
PKR:VenusC-ter
PACT:VenusC-ter
NT
NT
SINV
250 kDa
DICER
100 kDa
PKR
55 kDa
GFP
35 kDa
25 kDa
SINV CP
Ponceau
D
BiFC+DAPI
BiFC+DAPI
N-terVenus:DICER WT
+
TRBP:VenusC-ter
N-terVenus:DICER N1
+
TRBP:VenusC-ter

Figure S4

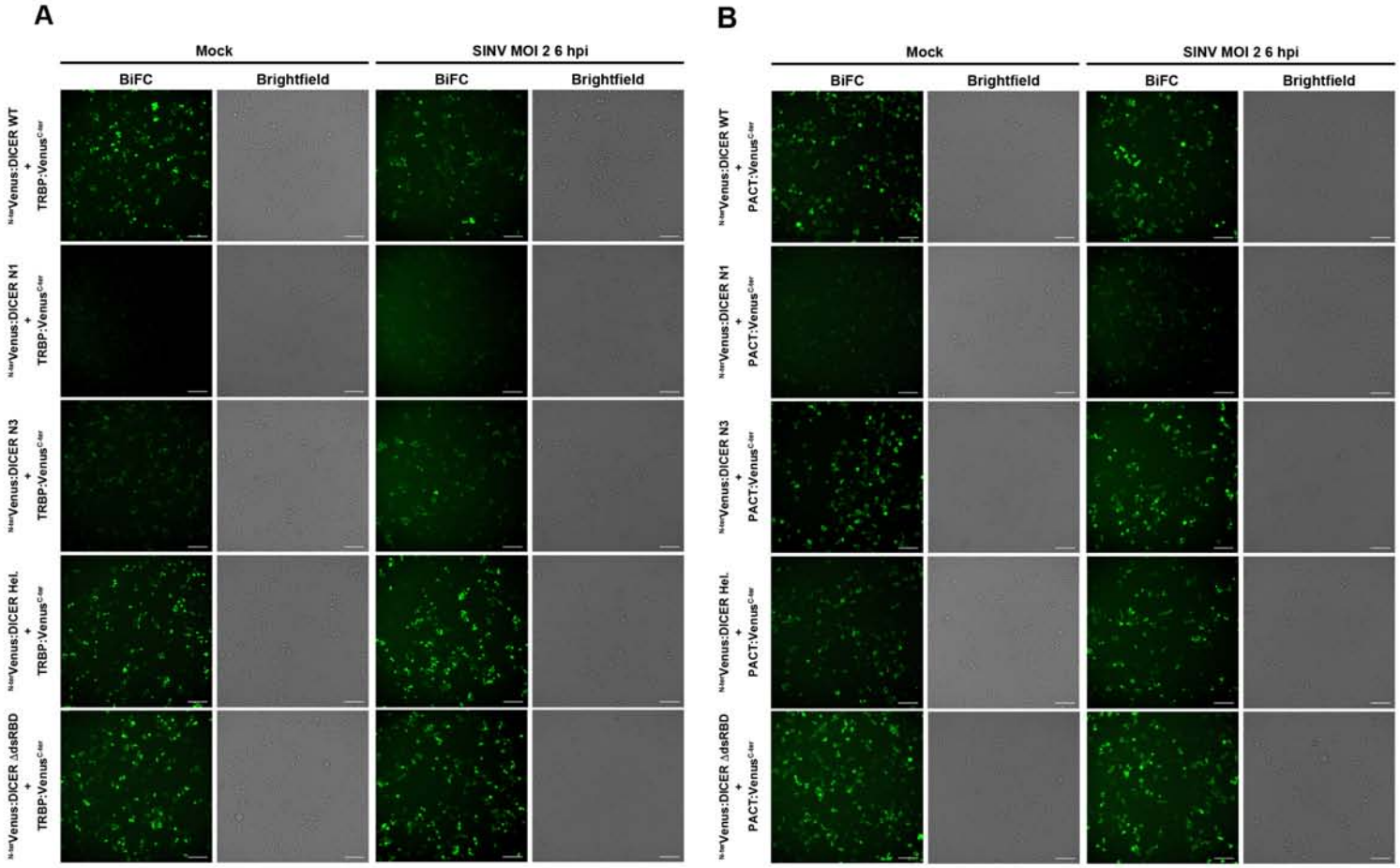
A
Mock
SINV MOI 2 6 hpi
BiFC
Brightfield
BiFC
Brightfield
N-terVenus:DICER WT + TRBP:VenusC-ter
N-terVenus:DICER N1 + TRBP:VenusC-ter
N-terVenus:DICER N3 + TRBP:VenusC-ter
N-terVenus:DICER Hel. + TRBP:VenusC-ter
N-terVenus:DICER ΔdsRBD + TRBP:VenusC-ter
B
Mock
SINV MOI 2 6 hpi
BiFC
Brightfield
BiFC
Brightfield
N-terVenus:DICER WT + PACT:VenusC-ter
N-terVenus:DICER N1 + PACT:VenusC-ter
N-terVenus:DICER N3 + PACT:VenusC-ter
N-terVenus:DICER Hel. + PACT:VenusC-ter
N-terVenus:DICER ΔdsRBD + PACT:VenusC-ter